Time-Coordinated Path Following of Multiple UAVs over Time-Varying Networks using $\mathcal{L}_1$ Adaptation

A. P. Aguiar and A. M. Pascoal
Instituto Superior Técnico, Torre Norte, Piso 8 Av. Rovisco Pais, 1 1049-001, Lisbon, Portugal
pedro@isr.ist.utl.pt antonio@isr.ist.utl.pt

I. Kaminer and V. Dobrokhodov
Naval Postgraduate School, Monterey, CA 93943, USA
kaminer@nps.edu vldobr@nps.edu

E. Xargay and N. Hovakimyan
University of Illinois at Urbana-Champaign, Urbana, IL 61801, USA
xargay@illinois.edu nhovakim@illinois.edu

ABSTRACT

Motivated by challenging mission scenarios, this paper tackles the problem of multi-Unmanned Aerial Vehicle (UAV) cooperative control in the presence of time-varying communication networks. Specifically, we address the problem of steering a fleet of UAVs along given paths (path following) so as to meet spatial and/or temporal constraints. One possible scenario is the situation where a fleet of vehicles is tasked to execute collision-free maneuvers under strict spatial constraints and arrive at their final destinations at exactly the same time. The paper builds on previous work by the authors on coordinated path following and extends it to allow for time-varying communication topologies.

Path following control in 3D builds on a nonlinear control strategy that is first derived at the kinematic level (outer-loop control). This is followed by the design of an $\mathcal{L}_1$ adaptive output feedback control law that effectively augments an existing autopilot and yields an inner-outer loop control structure with guaranteed performance. Multiple vehicle time-critical coordination is achieved by enforcing temporal constraints on the speed profiles of the vehicles along their paths in response to information exchanged over a dynamic communication network. We address explicitly the situation where each vehicle transmits its coordination state to only a subset of the other vehicles, as determined by the communications topology adopted. Further, we consider the case where the communication graph that captures the underlying communication network topology may be disconnected during some interval of time (or may even fail to be connected at any instant of time) and provide conditions under which the complete coordinated path following closed-loop system is stable. Hardware-in-the-Loop (HITL) simulation results demonstrate the benefits of the developed algorithms.

1.0 INTRODUCTION

Unmanned Aerial Vehicles (UAVs) are becoming ubiquitous and play an increasingly important role in military reconnaissance and strike operations, border patrol missions, forest fire detection, police surveillance, and

recovery operations, to name but a few. In simple applications, a single autonomous vehicle can be managed by a crew using a ground station provided by the vehicle manufacturer. The execution of more challenging missions, however, requires the use of multiple vehicles working in cooperation to achieve a common objective. Representative examples of cooperative mission scenarios are sequential auto-landing and coordinated ground target suppression for multiple UAVs. The first refers to the situation where a fleet of UAVs must break up and arrive at the assigned glideslope point, separated by pre-specified safe-guarding time-intervals. In the case of ground target suppression, a formation of UAVs must again break up and execute a coordinated maneuver to arrive at a predefined position over the target at the same time.

In both cases, no absolute temporal constraints are given *a priori* - a critical point that needs to be emphasized. Furthermore, the vehicles must execute maneuvers in close proximity to each other. In addition, as pointed out in Refs. [1, 2], the flow of information among vehicles may be severely restricted, either for security reasons or because of tight bandwidth limitations. As a consequence, no vehicle will be able to communicate with the entire formation and the inter-vehicle communication network may change over time. Under these circumstances, it is important to develop coordinated motion control strategies that can yield robust performance in the presence of time varying communication networks arising from communication failures and switching communication topologies.

Motivated by these and similar problems, over the past few years there has been increasing interest in the study of multi-agent system networks with application to engineering and science problems. The range of topics addressed include parallel computing [3], synchronization of oscillators [4], study of collective behavior and flocking [5], multi-system consensus mechanisms [6], multi-vehicle system formations [7], coordinated motion control [8] , asynchronous protocols [9], dynamic graphs [10], stochastic graphs [10–12], and graph-related theory [2, 13]. Especially relevant are the applications of the theory developed in the area of multi-vehicle formation control: spacecraft formation flying [14], unmanned aerial vehicle (UAV) control [15, 16], coordinated control of land robots [8], and control of multiple autonomous underwater vehicles (AUVs) [17, 18] . In spite of significant progress in these challenging areas, much work remains to be done to develop strategies capable of yielding robust performance of a fleet of vehicles in the presence of complex vehicle dynamics, communication constraints, and partial vehicle failures.

In Ref. [19], a general framework for the problem of coordinated control of multiple autonomous vehicles that must operate under strict spatial and temporal constraints was presented. The framework proposed borrows from multiple disciplines and integrates algorithms for path generation, path following, time-critical coordination, and $\mathcal{L}_1$ adaptive control theory for fast and robust adaptation. Together, these techniques yield control laws that meet strict performance requirements in the presence of modeling uncertainties and environmental disturbances. The methodology proposed in Ref. [19] is exemplified for the case of UAVs and unfolds in three basic steps. First, given a multiple vehicle task, a set of feasible trajectories is generated for all UAVs using an expedite method that takes explicitly into account the initial and final boundary conditions, a general performance criterion to be optimized, the simplified UAV dynamics, and safety rules for collision avoidance. The second step consists of making each vehicle follow its assigned path while tracking a desired speed profile. Path following control design is first done at a kinematic level, leading to an outer-loop controller that generates pitch and yaw rate commands to an inner-loop controller. The latter relies on off-the-shelf autopilots for angular rate command tracking, augmented with an $\mathcal{L}_1$ adaptive output feedback control law that guarantees stability and performance of the complete system for each vehicle in the presence of modeling uncertainties and environmental disturbances. Finally, in the third step the speed profile of each vehicle is adjusted about the nominal speed profile derived in the first step to enforce the temporal constraints that must be met in real-time in order to coordinate the entire fleet of UAVs. In this step, it is assumed that the vehicles exchange information over a fixed communication network.

The present paper builds on the work reported in Ref. [19] but departs considerably from it in that it allows for the consideration of time-varying communication networks. In particular, we address explicitly the case where the communication graph that captures the underlying communication network topology may be disconnected during some interval of time or may even fail to be connected at any instant of time. We show rigorously that if the desired speed profiles of the vehicles along their paths are constant and the connectivity of the communication graph satisfies a certain persistency of excitation (PE) condition, then the UAVs reach agreement. HITL simulation results demonstrate the benefits of the developed algorithms.

The paper is organized as follows. Section 3.0 presents a path following algorithm for UAVs in 3D space. At this stage, path following is done at the kinematic level (outer-loop control). Section 4.0 derives a strategy for time-coordinated control of multiple UAVs in the presence of time-varying communication topologies that relies on the adjustment of the desired speed profile of each vehicle. Section 5.0 describes an $\mathcal{L}_1$ adaptive augmentation technique both for path following and time coordination that yields an inner-loop control structure and exploits the availability of off-the-shelf autopilots. Sections 6.0 and 7.0 solve the problem of coordinated path following taking into account the UAV dynamics. Section 8.0 describes HILT simulation results and includes a brief description of the hardware used in the configuration. The paper ends with the conclusions in Section 9.0.

2.0 FEASIBLE PATH GENERATION FOR MULTIPLE AUTONOMOUS VEHICLES

Real-time path generation that explicitly accounts for the given boundary conditions and the dynamic constraints of the vehicle is a critical requirement for the autonomous vehicles of today. In this section, we describe an optimization algorithm for path generation that is suitable for real-time computation of feasible paths for multiple autonomous vehicles that guarantee collision avoidance and that can be followed by resorting to the path following algorithm proposed later in Section 3.0.

The key idea is to decouple space and time in the problem formulation from the beginning. This drastically reduces the number of optimization parameters and makes the real-time computational requirement easy to achieve. Intuitively, for example, if one chooses to make the vehicle's trajectory a function of the path length, the shape of the trajectory could be changed by increasing or decreasing this total length - a single optimization parameter. In addition, the vehicle's velocity and acceleration could be easily computed along this path. If the path length was too short, vehicle's velocity and acceleration would exceed the pre-specified bounds, thus making the trajectories infeasible - impossible for a vehicle to track given its dynamic constraints. This simple idea allows for computing feasible trajectories in real-time using a small number of optimization parameters.

To be more precise, consider a desired trajectory to be followed by a single vehicle and denote it by $p_c(\tau) = [x_1(\tau), x_2(\tau), x_3(\tau)]^\top$, which is parameterized by the virtual arc $\tau = [0; \tau_f]$, where τ_f is the total virtual arc length viewed as an optimization parameter. One particular way of representing the coordinates x_1, x_2, x_3 could be algebraic polynomials of degree N of the form $x_i(\tau) = \sum_{k=0}^{N} a_{ik}\tau^k,\ i = 1, 2, 3$, where the degree N of the polynomials $x_i(\tau)$ is determined by the number of boundary conditions that must be satisfied. Notice that these conditions (that involve spatial derivatives) are computed with respect to the parameter τ. There is an obvious need to relate them to actual temporal derivatives, but this issue will only be addressed later. For the time being, let d_0 and d_f be the highest-order of the spatial derivatives of $x_i(\tau)$ that must meet specified boundary constraints at the initial and final points of the path, respectively. Then, the minimum degree N^* of each polynomial is $N^* = d_0 + d_f + 1$. For example, if the desired path includes constraints on initial and final positions, velocities, and accelerations (second-order derivatives), then the degree of each polynomial is $N^* = 2 + 2 + 1 = 5$. Explicit formulae for computing boundary conditions $p_c'(0), p_c''(0)$ and $p_c'(\tau_f), p_c''(\tau_f)$ are given later in this section. Additional degrees of freedom may be included by making $N > N^*$. As an

7^{th} order	
Boundary conditions	$x_i(0), x_i'(0), x_i''(0), x_i'''(0), x_i(\tau_f), x_i'(\tau_f), x_i''(\tau_f), x_i'''(\tau_f),$
d_0/d_f	3/3
N^*/N	5/7

Linear algebraic matrix equation to solve for the coefficients a_{ik}

$$\begin{bmatrix} 1 & 0 & 0 & 0 & 0 & 0 & 0 & 0 \\ 0 & 1 & 0 & 0 & 0 & 0 & 0 & 0 \\ 0 & 0 & 2 & 0 & 0 & 0 & 0 & 0 \\ 1 & \tau_f & \tau_f^2 & \tau_f^3 & \tau_f^4 & \tau_f^5 & \tau_f^6 & \tau_f^7 \\ 0 & 1 & 2\tau_f & 3\tau_f^2 & 4\tau_f^3 & 5\tau_f^4 & 6\tau_f^5 & 7\tau_f^6 \\ 0 & 0 & 2 & 6\tau_f & 12\tau_f^2 & 20\tau_f^3 & 30\tau_f^4 & 42\tau_f^5 \\ 0 & 0 & 0 & 6 & 24\tau_f & 60\tau_f^2 & 120\tau_f^3 & 210\tau_f^4 \end{bmatrix} \begin{bmatrix} a_{i0} \\ a_{i1} \\ a_{i2} \\ a_{i3} \\ a_{i4} \\ a_{i5} \\ a_{i6} \\ a_{i7} \end{bmatrix} = \begin{bmatrix} x_i(0) \\ x_i'(0) \\ x_i''(0) \\ x_i'''(0) \\ x_i(\tau_f) \\ x_i'(\tau_f) \\ x_i''(\tau_f) \\ x_i'''(\tau_f) \end{bmatrix}$$

Table 1: Example of computation of the coefficients of a 7^{th} order polynomial path.

illustrative example, Table 1 shows how to compute the polynomial coefficients for polynomial trajectories of 7^{th} order, where additional constraints on the fictitious initial and final jerk (third-order derivatives) are included.

Parameterizing the desired path $p_c(\tau)$ by the virtual arc length τ provides additional flexibility. If one chooses $\tau = t$, then defining spatial profiles implies defining speed profiles along a given path as well. This is due to the fact that the vehicle speed along the path is related to the time derivatives of the path coordinates as $v(t) = \sqrt{\dot{x}_1^2(t) + \dot{x}_2^2(t) + \dot{x}_3^2(t)}$.

Next, one can define a *feasible* path as the one that can be followed by a vehicle without having it exceed prespecified bounds on the vehicle velocity $v_c(t)$ along the corresponding path, as well as on the total acceleration. Let $v_{\min}, v_{\max}$ and $a_{\max}$ denote predefined bounds on the vehicles velocity and total acceleration, respectively. Further letting $\eta(\tau) = d\tau/dt$, a path $p_c(\tau)$ is said to be *feasible*, if the following conditions are met:

$$v_{d_{\min}} \leq \eta(\tau)\ ||p_c'(\tau)|| \leq v_{d_{\max}},\ \ ||p_c''(\tau)\eta^2(\tau) + p_c'(\tau)\eta'(\tau)\eta(\tau)|| \leq a_{\max},\ \ \forall \tau \in [0, \tau_f], \tag{1}$$

where $p_c'(\tau), p_c''(\tau)$ are the first and second partials of $p_c(\tau)$ with respect to τ. In case of polynomial paths, $\eta(\tau)$ can be chosen as a polynomial of a degree sufficiently high to satisfy the boundary conditions on speed and acceleration. A *feasible path* can be obtained by solving, for example, the following optimization problem

$$F1 : \{\min_{\Xi_i} J(\cdot) \quad \text{subject to (1)},$$

where $J(\cdot)$ is a given cost function, such as final time, fuel consumption, down range, etc., and Ξ_i is the vector of optimization parameters, which includes τ_{f_i}, curvature and torsion of the i^{th} feasible path.

In this paper, we focus on time-critical missions that require that each vehicle follows a collision-free path and that all vehicle arrive at their respective destinations at the same time. We propose to address generation of collision free paths using two complementary approaches. The first one, referred to as deconfliction in time, guarantees that no two agents can be at the same place at the same time. Alternatively, the second approach – deconfliction in space - guarantees that no feasible paths intersect. The first approach relies on inter-vehicle communications and is thus a function of the quality of service (QoS) of the underlying network. On the other

hand, the second approach may be particularly useful in military applications, where jamming prevents vehicles from communicating with each other and is infinitely preferable to the current practice of separating vehicles by altitude. Formally these approaches lead to the following constraints.

Deconfliction-in-time:

$$\min_{j,k=1,\ldots,n,j\neq k} ||p_c^j(t) - p_c^k(t)||^2 \geq E^2 \text{ for any } t \in [0, t_f],$$

Deconfliction in space:

$$\min_{j,k=1,\ldots,n,j\neq k} ||p_c^j(\tau_j) - p_c^k(\tau_k)||^2 \geq E^2 \text{ for any } \tau_j, \tau_k \in [0, \tau_{fj}] \times [0, \tau_{fk}].$$

where $t_f = \int_0^{\tau_{fi}} \frac{d\tau}{\eta_i(\tau)}$ for any $i \in [1, \cdots, n]$, and E is the distance for spatial clearance. Notice that t_f is subject to $t_f \leq T_f$, where T_f is the predefined upper bound on the final time for the missions to be completed.

In addition to the collision avoidance, the simultaneous time-of-arrival requirement introduces an additional constraint on the path lengths of the vehicles. Letting $T_i = [t_{fi_{\min}}, t_{fi_{\max}}]$ be the arrival time interval for the i^{th} vehicle, where the minimum $t_{fi_{\min}}$ and maximum $t_{fi_{\max}}$ can be computed using the lower and upper bounds on the velocity of the i^{th} vehicle, the simultaneous arrival problem has a solution *if and only if* $T_i \bigcap T_j \neq \emptyset \, \forall i, j = 1, \ldots, n, i \neq j$. This is guaranteed if the *arrival margin*, defined as $\mathcal{T} = \min_i t_{fi_{\max}} - \max_i t_{fi_{\min}}$ is strictly positive, Fig. 2 (left).

Letting $J(\cdot)$ be the cost function to be minimized, the first optimization problem addresses the deconfliction in time:

$$F2: \begin{cases} \min\limits_{\Xi_1 \times \cdots \times \Xi_n} J(\cdot) \text{ subject to (1) for any } i \in [1, n] \text{ and} \\ \min\limits_{j,k=1,\ldots,n,j\neq k} ||p_c^j(t) - p_c^k(t)||^2 \geq E^2(\gamma, \mu) \text{ for any } t \in [0, t_f], \\ \mathcal{T} \geq \mathcal{T}_0 > 0\,, \\ t_f \ < \ T_f\,, \end{cases} \tag{2}$$

where Ξ_i includes τ_{fi}, the torsion and the curvature of the feasible paths, and $E(\gamma, \mu)$ represents the minimum allowable separation distance between the paths that is a function of the path following controller performance γ and also of the QoS of the underlying network, defined as μ. Clearly, as QoS decreases, $E(\gamma, \mu)$ should increase.

The second optimization problem, which we will address in the present paper, accounts for the deconfliction in space:

$$F3: \begin{cases} \min\limits_{\Xi_1 \times \cdots \times \Xi_n} J(\cdot) \text{ subject to (1) for any } i \in [1, n] \text{ and} \\ \min\limits_{j,k=1,\ldots,n,j\neq k} ||p_c^j(\tau_j) - p_c^k(\tau_k)||^2 \geq E^2(\gamma) \text{ for any } \tau_j, \tau_k \in [0, \tau_{fj}] \times [0, \tau_{fk}], \\ \mathcal{T} \geq \mathcal{T}_0 > 0\,, \\ \int_0^{\tau_{fi}} \frac{d\tau}{\eta_i(\tau)} \ < \ T_f\,, \ \ i = 1, \ldots, n\,, \end{cases} \tag{3}$$

where $\mathcal{T} \geq \mathcal{T}_0 > 0$ imposes a bounded away from zero arrival margin requirement, Ξ_i is the set of optimization parameters for the i^{th} vehicle and $E(\gamma)$ represents the minimum allowable separation distance between the paths and is a function of the path following controller performance γ.

In this paper we are interested in small UAVs that operate essentially at constant speeds. Clearly, in this case speed constraints can be easily satisfied for any constant $v_p \in [v_{d_{\min}}, v_{d_{\max}}]$. This in turn defines

$$\eta(\tau) = \frac{v_p}{||p_c'(\tau)||} \tag{4}$$

$$\dot{p}_c(t) = v_p \frac{p_c'(\tau)}{||p_c'(\tau)||} \tag{5}$$

$$\ddot{p}_c(t) = \frac{v_p^2}{||p_c'(\tau)||^2}(I - \frac{p_c'(\tau)(p_c'(\tau))^T}{||p_c'(\tau)||^2})p''(\tau)\,. \tag{6}$$

Therefore, we can choose

$$p_c'(0) = \frac{\dot{p}_c(0)}{||\dot{p}_c(0)||} \tag{7}$$

$$p_c'(\tau_f) = \frac{\dot{p}_c(t_f)}{||\dot{p}_c(t_f)||}. \tag{8}$$

to satisfy boundary conditions on $\dot{p}_c(t)$. Similarly, setting

$$\begin{aligned} p_c''(0) &= \ddot{p}_c(0) \\ p_c''(\tau_f) &= \ddot{p}_c(t_f), \end{aligned}$$

satisfies equation (6) at the boundaries.

Since in this paper we consider the scenario in which a fleet of UAVs is tasked to arrive at their final destinations at exactly the same time, the generated paths should be designed in such a way as to guarantee the simultaneous arrival by all UAVs at their respective destinations. Next, we make these ideas more precise.

Let l_{fi} denote the total path length of the ith path and v_{p_i} denote its velocity along this path. Then

$$l_{fi} = \int_0^{\tau_{fi}} ||p_{c_i}'(\tau_i)||\, d\tau_i.$$

It follows immediately that the time of flight t_{fi} of UAV i is given by

$$t_{fi_{\min}} = \int_0^{\tau_{fi}} \frac{||p_{c_1}'(\tau_i)||}{v_{\mathrm{p}_i}}\, d\tau_i.$$

Define a cost function $J = (\max_i t_{fi} - \min_i t_{fi})$. Then, making J arbitrarily small over the set of feasible paths, feasible velocities and accelerations will result in the desired solution to the simultaneous arrival problem discussed above. Therefore, we propose to solve the path generation problem $F3$ with this cost function J.

The optimization problem $F3$ can be effectively solved in real-time by adding a penalty function G as discussed in Ref. [20] and by using any zero-order optimization technique. As an example, Fig. 1 illustrates the flexibility afforded by the reference polynomials to compute a coordinated target reconnaissance mission by three UAVs. In this case, the vector of optimization parameters is $\Xi = [\tau_{f1}\ \tau_{f2}\ \tau_{f3}\ v_{p_1}\ v_{p_2}\ v_{p_3}]$. The final value of the cost function $J = 1.6968e-006$ corresponds to $|\max_i t_{fi} - \min_i t_{fi}| \leq\ 0.0013\ \ sec.$ The value

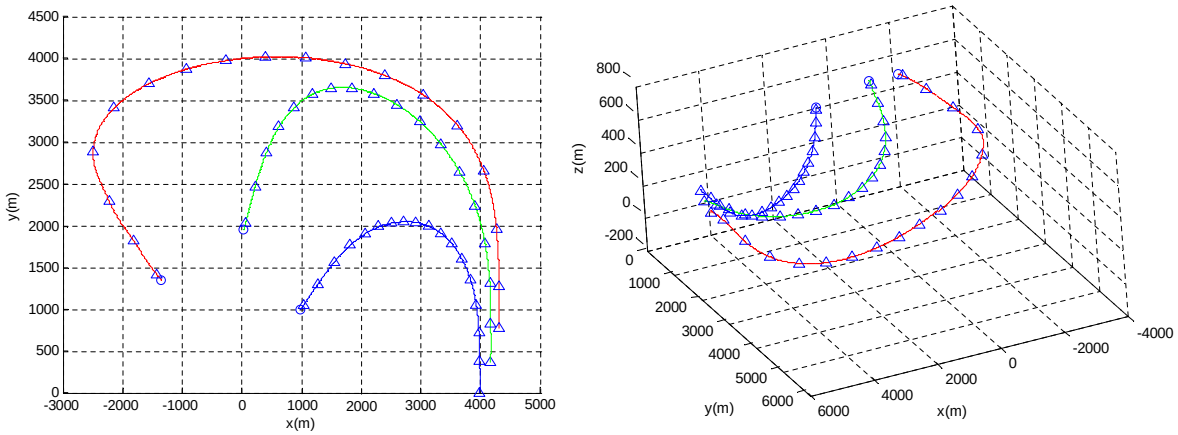

Figure 1: Example of spatially deconflicted trajectories. Top view, moving from right to left (left), 3D view, moving from left to right (right).

of the optimization parameter vector $\Xi_{final} = [4010.0 \;\; 4999.7 \;\; 7487.6 \;\; 15.1380 \;\; 21.2238 \;\; 29.8054]$ resulted in spatially deconflicted paths where the minimum distance between any two paths did not fall below $350\ m$ (the minimum required distance was $100\ m$). The optimal speed profiles $[15.1380\ m/s \;\; 21.2238\ m/s \;\; 29.8054\ m/s]$ are well within predefined limits of $v_{\min}, v_{\max}$ were $15m/sec$ and $30m/sec$, respectively. The maximum acceleration corresponding to each path did not exceed $0.89m/sec^2$, well below the limit of $0.5g$. Finally, the resulting total path lengths for each path were $[l_{f1} \;\; l_{f2} \;\; l_{f3}] = [4535.4 \;\; 6358.7 \;\; 8929.7]$.

The outcome of the optimization problem $F3$ will include the desired path and velocity assignment for each vehicle, such that if every vehicle follows these commanded paths and speed profiles, the time-critical mission(s) will be successfully executed in the ideal case. However, the presence of disturbances, modeling uncertainties and failures in the communication network require synthesis of *robust* feedback laws to ensure that the mission can be accomplished with a certain degree of confidence. The remaining sections propose a framework to synthesize path following and time-coordination control laws that address the performance of the overall time-critical mission in the presence of uncertainty and over a faulty, time-varying communication network.

3.0 PATH FOLLOWING IN 3D SPACE

This section describes an algorithm for UAV path following in 3D space. In order for the ith vehicle to follow the spatial path $p_{c_i}(\tau)$, a path following algorithm that extends the one in Ref.[21] to a 3D setting with a further modification aimed at meeting time-critical and inter-vehicle constraints is now presented. At this level, only the simplified kinematic equations of the vehicle will be addressed by taking pitch rate and yaw rate as virtual outer-loop control inputs. The dynamics of the closed-loop UAV with autopilot are dealt with in Sections 6.0 and 7.0 by introducing an inner-loop control law via the novel $\mathcal{L}_1$ adaptive output feedback controller.

Figure 3 captures the geometry of the problem at hand. Let $\mathcal{I}$ denote an inertial frame. Let Q be the UAV center of mass. Further, let $p_c(l)$ be the path to be followed, parameterized by its path length l, and P be an arbitrary point on the path that plays the role of the center of mass of a virtual UAV to be followed. Note that this is a different approach as compared to the set-up for path following originally proposed in Ref.[22] , where P was simply defined as the point on the path that is closest to the vehicle. Endowing P with an extra degree

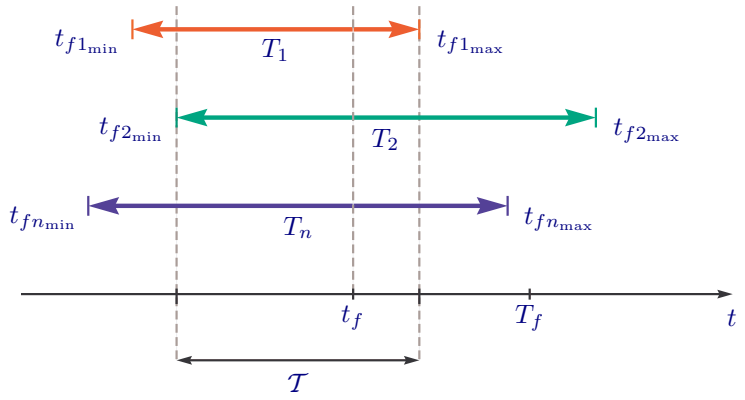

Figure 2: Intersection of time intervals T_i for each UAV.

of freedom is the key to the algorithm presented in Ref.[21].

Let $\mathcal{F}$ be a Serret-Frenet frame attached to the point P on the path, and let $T(l)$, $N(l)$ and $B(l)$ be an orthonormal basis for $\mathcal{F}$. We recall that these unit vectors define the tangent, normal, and binormal directions, respectively to the path at the point determined by l. They can be used to construct the rotation matrix $R_F^I = [T\ N\ B]$ from $\mathcal{F}$ to $\mathcal{I}$. Denote by ω_{FI}^F the angular velocity of $\mathcal{F}$ with respect to $\mathcal{I}$, resolved in $\mathcal{F}$. Let

$$q_I(t) \quad = \quad [x_I(t)\ y_I(t)\ z_I(t)]^\top$$

be the position of the UAV center of mass Q resolved in $\mathcal{I}$, and let

$$q_F(t) \quad = \quad [x_F(t)\ y_F(t)\ z_F(t)]^\top$$

be the difference between $q_I(t)$ and $p_c(t)$ resolved in $\mathcal{F}$. Finally, let $\mathcal{W}'$ denote a coordinate system defined by projecting the wind frame $\mathcal{W}$ onto a local level plane. (The frame $\mathcal{W}$ has its origin at Q and its x-axis is aligned with the UAV's velocity vector).

Let

$$\Phi_e(t) \quad = \quad [\phi_e(t)\ \theta_e(t)\ \psi_e(t)]^\top$$

denote the Euler angles that locally parameterize the rotation matrix from $\mathcal{F}$ to $\mathcal{W}'$. In what follows, $v(t)$ is the magnitude of the UAV's velocity vector, $\gamma(t)$ is the flight path angle, $\psi(t)$ is the ground heading angle, and $q(t)$ and $r(t)$ are the y-axis and z-axis components, respectively, of the vehicle's rotational velocity resolved in $\mathcal{W}'$ frame. For the purpose of this paper and with a slight abuse of notation, $q(t)$ and $r(t)$ will be referred to as *pitch rate* and *yaw rate*, respectively, in the $\mathcal{W}'$ frame.

Straightforward computations[1] yield the dynamic equations of the path following kinematic error states as

$$\mathcal{G}_e \quad : \quad \begin{cases} \dot{x}_F = -\dot{l}(1-\kappa(l)y_F) + v\cos\theta_e\cos\psi_e \\ \dot{y}_F = -\dot{l}(\kappa(l)x_F - \zeta(l)z_F) + v\cos\theta_e\sin\psi_e \\ \dot{z}_F = -\dot{l}\zeta(l)y_F - v\sin\theta_e \\ \begin{bmatrix} \dot{\theta}_e \\ \dot{\psi}_e \end{bmatrix} = D\left(t,\theta_e,\psi_e\right) + T\left(t,\theta_e\right)\begin{bmatrix} q \\ r \end{bmatrix} \end{cases} \tag{9}$$

[1] See Ref.[23] for details in the derivation of these dynamics.

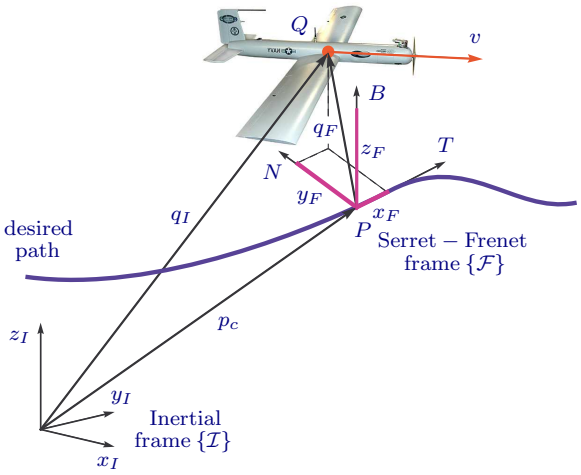

Figure 3: Problem geometry

where

$$D\left(t,\theta_e,\psi_e\right) = \begin{bmatrix} \dot{l}\zeta(l)\sin\psi_e \\ -\dot{l}(\zeta(l)\tan\theta_e\cos\psi_e + \kappa(l)) \end{bmatrix} \tag{10}$$

$$T\left(t,\theta_e\right) = \begin{bmatrix} \cos\phi_e & -\sin\phi_e \\ \frac{\sin\phi_e}{\cos\theta_e} & \frac{\cos\phi_e}{\cos\theta_e} \end{bmatrix}. \tag{11}$$

and with $\kappa(l) = \left\| \frac{dT(l)}{dl} \right\|$ being the curvature of the path and $\zeta(l) = \left\| \frac{dB(l)}{dl} \right\|$ being its torsion.

Note that, in the kinematic error model (9), $q(t)$ and $r(t)$ play the role of "virtual" control inputs. Notice also how the rate of progression $\dot{l}(t)$ of the point P along the path becomes an extra variable that can be manipulated at will.

At this point, it is convenient to formally define the state vector for the path following kinematic dynamics as

$$x(t) = \begin{bmatrix} x_F(t) & y_F(t) & z_F(t) & \theta_e(t) - \delta_\theta(t) & \psi_e(t) - \delta_\psi(t) \end{bmatrix}^\top,$$

where

$$\begin{aligned} \delta_\theta(t) &= \sin^{-1}\left(\frac{z_F(t)}{|z_F(t)| + d_1}\right), \\ \delta_\psi(t) &= \sin^{-1}\left(\frac{-y_F(t)}{|y_F(t)| + d_2}\right), \end{aligned} \tag{12}$$

with d_1 and d_2 being some positive constants. Notice that, instead of the angular errors $\theta_e(t)$ and $\psi_e(t)$, we use $\theta_e(t) - \delta_\theta(t)$ and $\psi_e(t) - \delta_\psi(t)$ respectively to shape the "approach" angles to the path. Clearly, when the vehicle is far from the desired path the approach angles become close to $\pi/2$. As the vehicle comes closer to the path, the approach angles tend to 0. The system $\mathcal{G}_e$ is completely characterized by defining the vector of

input signals as

$$y(t) \;=\; [\; q(t) \quad r(t) \;]^\top .$$

Next, we show that there exist stabilizing functions for $q(t)$ and $r(t)$ leading to local exponential stability of the origin of $\mathcal{G}_e$ with a prescribed domain of attraction. We start by assuming that the UAV speed satisfies the lower bound

$$v_{\min} \;\leq\; v(t)\,, \qquad \forall\, t \geq 0\,. \tag{13}$$

Let c_1 and c_2 be arbitrary positive constants satisfying the following condition

$$\nu_i \triangleq \sqrt{cc_2} + \sin^{-1}\left(\frac{\sqrt{cc_1}}{\sqrt{cc_1}+d_i}\right) \;\leq\; \frac{\pi}{2} - \epsilon_i\,, \;\; i=1,2 \tag{14}$$

where $c>0$ is any positive constant, d_1 and d_2 were introduced in (12), and ϵ_1 and ϵ_2 are positive constants such that $0<\epsilon_i<\frac{\pi}{2},\ i=1,2$. Let the rate of progression of the point P along the path be governed by

$$\dot{l}(t) \;=\; K_1 x_F(t) + v(t)\cos\theta_e(t)\cos\psi_e(t)\,, \tag{15}$$

where $K_1>0$. Then, the input vector $y_c(t)$ given by

$$y_c(t) \;=\; \left[\begin{array}{c} q_c(t) \\ r_c(t) \end{array}\right] \;=\; T^{-1}\left(t,\theta_e\right)\left(\left[\begin{array}{c} u_{\theta_c}(t) \\ u_{\psi_c}(t) \end{array}\right] - D\left(t,\theta_e,\psi_e\right)\right), \tag{16}$$

where $D\left(t,\theta_e,\psi_e\right)$ and $T\left(t,\theta_e\right)$ were introduced in (10) and (11), and $u_{\theta_c}(t)$ and $u_{\psi_c}(t)$ are defined as

$$\begin{aligned} u_{\theta_c}(t) \;&=\; -K_2\left(\theta_e(t)-\delta_\theta(t)\right) + \frac{c_2}{c_1} z_F(t) v(t) \frac{\sin\theta_e(t)-\sin\delta_\theta(t)}{\theta_e(t)-\delta_\theta(t)} + \dot{\delta}_\theta(t) \\ u_{\psi_c}(t) \;&=\; -K_3\left(\psi_e(t)-\delta_\psi(t)\right) - \frac{c_2}{c_1} y_F(t) v(t)\cos\theta_e(t) \frac{\sin\psi_e(t)-\sin\delta_\psi(t)}{\psi_e(t)-\delta_\psi(t)} + \dot{\delta}_\psi(t)\,, \end{aligned} \tag{17}$$

stabilizes the subsystem $\mathcal{G}_e$ for any $K_2>0$ and $K_3>0$. Figure 4 presents the kinematic closed-loop system. A formal statement of this key result is given in the lemma below.

Lemma 1 *Let $d=\sqrt{cc_1}$, where c and c_1 were introduced in (14). Further, let the progression of the point P along the path be governed by (15). Then, for any $v(t)$ verifying (13), the origin of the kinematic error equations in (9) with the controllers $q(t)\equiv q_c(t)$, $r(t)\equiv r_c(t)$ defined in (16)-(17) is exponentially stable with the domain of attraction*

$$\Omega \;=\; \left\{x \;:\; V_p(x) < \frac{c}{2}\right\}, \tag{18}$$

where

$$\begin{aligned} V_p(x) \;&=\; x^\top P_p x \\ P_p \;&=\; \mathrm{diag}\left(\frac{1}{2c_1},\frac{1}{2c_1},\frac{1}{2c_1},\frac{1}{2c_2},\frac{1}{2c_2}\right). \end{aligned}$$

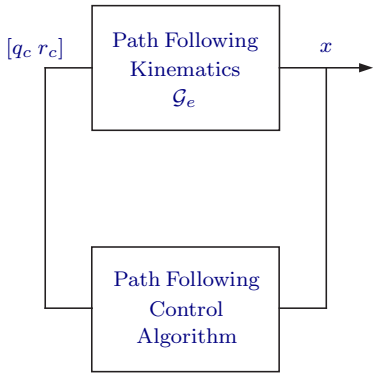

Figure 4: Path following closed-loop system for a single UAV solved at a kinematic level

Proof. If $q(t) \equiv q_c(t)$ and $r(t) \equiv r_c(t)$, it is easy to check from (9) and (16) that

$$\begin{aligned} \dot{\theta}_e(t) &= u_{\theta_c}(t), \\ \dot{\psi}_e(t) &= u_{\psi_c}(t)\,. \end{aligned}$$

Then, it follows from (9), (12), (15), and (16)-(17) that

$$\dot{V}_p = -x^\top Q_p x\,,$$

with

$$Q_p = \mathrm{diag}\left(\frac{K_1}{c_1}\ \frac{v\cos\theta_e}{c_1(|y_F|+d_2)}\ \frac{v}{c_1(|z_F|+d_1)}\ \frac{K_2}{c_2}\ \frac{K_3}{c_2}\right). \tag{19}$$

Note that over the compact set Ω the following upper bounds hold

$$\begin{aligned} |x_F(t)| &< d, \\ |y_F(t)| &< d, \\ |z_F(t)| &< d, \\ |\theta_e(t)| &< \sqrt{cc_2} + |\delta_\theta(t)| < \sqrt{cc_2} + \sin^{-1}\left(\frac{d}{d+d_1}\right) = \nu_1 < \frac{\pi}{2}, \\ |\psi_e(t)| &< \sqrt{cc_2} + |\delta_\psi(t)| < \sqrt{cc_2} + \sin^{-1}\left(\frac{d}{d+d_2}\right) = \nu_2 < \frac{\pi}{2}\,, \end{aligned} \tag{20}$$

where we have used the relationship (14). Now it follows from (19) and (20) that $Q_p \geq \bar{Q}_p$, where

$$\bar{Q}_p = \mathrm{diag}\left(\frac{K_1}{c_1}\ \frac{v_{\min}\cos\nu_1}{c_1(d+d_2)}\ \frac{v_{\min}}{c_1(d+d_1)}\ \frac{K_2}{c_2}\ \frac{K_3}{c_2}\right). \tag{21}$$

Since $\bar{Q}_p > 0$ and

$$\dot{V}_p(x) \leq -x^\top \bar{Q}_p x\,, \quad \forall\, t \geq 0\,,$$

$x(t)$ converges exponentially to zero over the compact set Ω. Then, it follows from the definitions in (12) that both $\delta_\theta(t)$ and $\delta_\psi(t)$ converge exponentially to zero, and thus one finds that $\theta_e(t)$ and $\psi_e(t)$ also converge exponentially to zero, which completes the proof.

A more detailed derivation of this proof can be found in Ref.[24]. □

Remark 1 *The control law* (16)-(17) *produces angular rate commands defined in $\mathcal{W}'$ frame. However, a typical commercial autopilot accepts rate commands defined in body-fixed frame $\mathcal{B}$. The coordinate transformation from $\mathcal{W}'$ to $\mathcal{B}$ is given by*

$$R^B_{W'} \;=\; R^B_W R^W_{W'}\,,$$

where the transformation R^B_W is defined using the angle of attack and the sideslip angle. For the UAVs considered in this paper, these angles are usually small, and therefore it is reasonable to assume that $R^B_W \approx \mathbb{I}$. On the other hand, $R^W_{W'}$ is defined via a single rotation around a local x-axis by an angle ϕ_W. For small values of angle of attack and sideslip angle, ϕ_W can be approximated by the body-fixed bank angle ϕ measured by a typical autopilot. Therefore, in the final implementation, the angular rate commands (16)-(17) *are resolved in the body-fixed frame $\mathcal{B}$ using the transformation discussed here.*

Thus, in the following sections we assume that both the autopilot angular rates $y(t) = [q(t)\; r(t)]^\top$ and the commanded angular rates $y_c(t) = [q_c(t)\; r_c(t)]^\top$ are resolved in $\mathcal{W}'$. We notice that this assumption will not affect the results since, for small angle of attack and sideslip angle, we have

$$\|(y(t) - y_c(t))^{W'}\|_2 \;\approx\; \|(y(t) - y_c(t))^{B}\|_2\,.$$

4.0 TIME-CRITICAL COORDINATION

Having solved the path following problem for a single vehicle and an arbitrary speed profile at a kinematic level, we now address the problem of time-coordinated control of multiple vehicles. Examples of applications in which this would be useful include situations where all vehicles must arrive at their final destinations at exactly the same time, or at different times so as to meet a desired inter-vehicle arrival schedule. Without loss of generality, we consider the problem of simultaneous arrival. Let t_f be the arrival time of the first UAV. Denote l_{f_i} as the total length of the spatial path for the ith UAV. In addition, let $l_i(t)$ be the path length from the origin to $p_i(t)$ along the spatial path of the ith UAV. Define $l'_i(t) = l_i(t)/l_{fi}$. Clearly, $l'_i(t_f) = 1$ for $i = 1, 2, \ldots, n$ implies that all vehicles arrive at their final destination at the same time. Since $\dot{l}'_i(t) = \dot{l}_i(t)/l_{fi}$, it follows from (15) that

$$\dot{l}'_i(t) \;=\; \frac{K_1 x_{F_i}(t) + v_i(t)\cos\theta_{e,i}(t)\cos\psi_{e,i}(t)}{l_{fi}}\,, \tag{22}$$

where for simplicity we have kept K_1 without indexing.

To account for the communication constraints, we introduce the neighborhood set J_i that denotes the set of vehicles that the ith vehicle exchanges information with. We impose the constraint that each UAV only exchanges its coordination parameter $l'_i(t)$ with its neighbors according to the topology of the communications.

Then, to solve the coordination problem, we propose the following desired speed profile for the ith UAV [23]

$$v_{c_i}(t) \;=\; \frac{u_{\mathrm{coord}_i}(t) l_{fi} - K_1 x_{F_i}(t)}{\cos\theta_{e,i}(t)\cos\psi_{e,i}(t)}\,, \qquad i = 1, \ldots, n\,, \tag{23}$$

with the following decentralized coordination law

$$\begin{aligned} u_{\text{coord}_1}(t) &= -a\sum_{j\in J_1}(l_1'(t)-l_j'(t)) + \tfrac{v_{d_1}}{l_{f_1}} \\ u_{\text{coord}_i}(t) &= -a\sum_{j\in J_i}(l_i'(t)-l_j'(t)) + \chi_{I_i}(t)\,, \qquad i=2,\ldots,n \\ \dot{\chi}_{I,i}(t) &= -b\sum_{j\in J_i}(l_i'(t)-l_j'(t))\,, \quad \chi_{I_i}(0)=\tfrac{v_{d_i}}{l_{f_i}} \qquad i=2,\ldots,n \end{aligned}$$

where we have elected vehicle 1 as the formation leader, v_{d_1} denotes its desired constant speed profile, v_{d_i}, $i=2,\ldots,n$, is the speed profile of the follower vehicles, and a, b are positive constants. Note that the coordination control law has a Proportional-Integral (PI) structure, thus allowing each vehicle to learn the speed of the leader, rather than having it available *a priori*.

The coordination law can be re-written in compact form as

$$u_{\text{coord}}(t) = -aL(t)l'(t) + \begin{bmatrix} v_{d_1}/l_{f_1} \\ \chi_I(t) \end{bmatrix}, \tag{24}$$

$$\dot{\chi}_I(t) = -bC^\top L(t)l'(t), \quad \chi_{I_i}(0) = \frac{v_{d_i}}{l_{f_i}} \tag{25}$$

where $l'(t) = [l_1'(t)\ \ldots\ l_n'(t)]^\top$, $u_{\text{coord}}(t) = [u_{\text{coord}_1}(t)\ \ldots\ u_{\text{coord}_n}(t)]^\top$, $\chi_I(t) = [\chi_{I_2}(t)\ \ldots\ \chi_{I_n}(t)]^\top$, $C^\top = [\ 0 \quad I_{n-1}\ ]$, and the $n\times n$ piecewise-continuous matrix $L(t)$ can be interpreted as the Laplacian of an undirected graph $\Gamma(t)$ that captures the underlying bidirectional communication network topology of the UAV formation at time t. It is well known that $L^\top(t)=L(t)$, $L(t)\geq 0$, $L(t)1_n=0$, and that the second smallest eigenvalue of $L(t)$ is strictly positive, that is,

$$\min_{\substack{x\neq 0\\ 1_n^\top x=0}} \frac{x^\top L(t)x}{\|x\|^2} = \lambda_2(L(t)) > 0$$

if and only if the graph Γ is connected (see e.g., Ref.[25]).

In preparation for the development that follows, next we reformulate the coordination problem stated above into a stabilization problem. To this aim, we introduce the following notation: let

$$\Pi \triangleq \mathbb{I}_n - \frac{1_n 1_n^\top}{n}$$

denote the *projection matrix* and Q be a $(n-1)\times n$ matrix such that

$$Q1_n = 0, \quad QQ^\top = \mathbb{I}_{n-1}.$$

Notice that $Q^\top Q=\Pi$, $\Pi = \Pi^\top = \Pi^2$, $L(t)\Pi = \Pi L(t) = L(t)$, and the spectrum of the matrix $\bar{L}(t)\triangleq QL(t)Q^\top$ is equal to the spectrum of $L(t)$ without the eigenvalue $\lambda=0$ correspondent to the eigenvector 1_n. Define the state variables $\zeta(t)=[\zeta_1(t)^\top\ \zeta_2(t)^\top]^\top$ as

$$\begin{aligned} \zeta_1(t) &= Q\,l'(t) \\ \zeta_2(t) &= \chi_I(t) - \frac{v_{d_1}(t)}{l_{f_1}}1_{n-1}\,, \end{aligned}$$

where by definition $\zeta_1(t) = 0 \Leftrightarrow l' \in \text{span}\{1_n\}$ which implies that, if $\zeta(t_f) = 0$, then all UAVs arrive at their final destination at the same time.

Thus, setting

$$e_{v_i}(t) \;=\; v_i(t) - v_{c_i}(t)\,, \qquad i = 1, \ldots, n\,,$$

where $e_{v_i}(t)$ denotes the velocity error for the ith vehicle in the coordination, it follows from (23) that the kinematic equation (22) can be rewritten as

$$\dot{l}'_i(t) \;=\; u_{\text{coord}_i}(t) + \frac{e_{v_i}(t)\cos\theta_{e,i}(t)\cos\psi_{e,i}(t)}{l_{fi}}\,, \tag{26}$$

and therefore, the closed-loop coordination dynamics formed by (26) and the coordination control algorithm defined in (24)-(25) can be reformulated as

$$\dot{\zeta}(t) \;=\; F(t)\zeta(t) + H\varphi(t)\,, \tag{27}$$

where

$$F(t) \;=\; \begin{bmatrix} -a\bar{L}(t) & QC \\ -bC^\top Q^\top \bar{L}(t) & 0 \end{bmatrix}$$

$$H \;=\; \begin{bmatrix} Q \\ 0 \end{bmatrix},$$

and $\varphi(t) \in \mathbb{R}^n$ is a vector with its ith element $\frac{e_{v_i}(t)\cos\theta_{e,i}(t)\cos\psi_{e,i}(t)}{l_{fi}}$.

Next we show that for fixed or time-varying communication topologies but assuming that the graph remains connected for all $t \geq 0$, if every vehicle travels at the commanded speed $v_{c_i}(t)$ ($e_{v_i}(t) \equiv 0$), then the coordinated system reaches agreement and all the vehicles travel at the same path length rate, that is

$$\lim_{t\to\infty}\left(l'_i(t) - l'_j(t)\right) \;=\; 0\,, \qquad \forall i, j \in \{1, \ldots, n\}$$

$$\lim_{t\to\infty} \dot{l}'(t) \;=\; \frac{v_{d_1}}{l_{f_1}}\,.$$

On the other hand, if $e_{v_i}(t) \neq 0$, then the error of the disagreement vector degrades gracefully with the size of $|e_{v_i}(t)|$.

Lemma 2 *Consider the coordination system* (27) *and suppose that the graph that models the communication topology $\Gamma(t)$ is connected for all $t \geq 0$. Then, for any selected rate of convergence $\bar{\lambda} > 0$, there exist sufficiently large coordinated control gains a, b such that the system* (27) *is input-to-state stable (ISS) with respect to $e_v(t) = [e_{v_1}(t) \;\cdots\; e_{v_n}]^\top$, that is,*

$$\|\zeta(t)\| \;\leq\; k_1\,\|\zeta(0)\|\,e^{-\bar{\lambda}t} + k_2 \sup_{\tau\in[0,t)} \|e_v(\tau)\|\,, \qquad \forall t \geq 0 \tag{28}$$

for some $k_1, k_2 > 0$. Furthermore, the normalized lengths $l'_i(t)$ and path-length rates $\dot{l}'_i(t)$ satisfy

$$\limsup_{t\to\infty} \left|l'_i(t) - l'_j(t)\right| \;\leq\; k_3 \limsup_{t\to\infty} \|e_v(t)\|\,, \tag{29}$$

$$\limsup_{t\to\infty} \left|\dot{l}'_i(t) - \frac{v_{d_1}}{l_{f_1}}\right| \;\leq\; k_4 \limsup_{t\to\infty} \|e_v(t)\|\,, \tag{30}$$

for all $i, j \in \{1, \ldots, n\}$, and for some $k_3, k_4 > 0$.

Proof. To prove ISS we first show that the homogeneous equation of the coordination dynamics

$$\dot{\zeta}(t) \;=\; F(t)\zeta(t) \tag{31}$$

is uniformly exponentially stable. To this aim, we consider the Lyapunov function candidate

$$V_c(\zeta(t)) \;=\; \zeta^\top(t) P_c \zeta(t) \tag{32}$$

where P_c is defined to have the following structure

$$P_c \;=\; \begin{bmatrix} \mathbb{I}_{n-1} & -\frac{\delta}{2\bar{\lambda}n^2} QC \\ -\frac{\delta}{2\bar{\lambda}n^2} C^\top Q^\top & \frac{a\delta}{2b\bar{\lambda}n^2}\mathbb{I}_{n-1} \end{bmatrix}, \tag{33}$$

with $\delta > 0$ being an arbitrary positive constant yet to be defined.

We notice now that, since the graph $\Gamma(t)$ is connected for every $t \geq 0$, it follows that there exists a constant $\delta_c > 0$ such that

$$\lambda_2(L(t)) > \delta_c, \quad \forall t \geq 0\,. \tag{34}$$

If we set $\delta = \delta_c$ in the definition of P_c in (33), then the lower bound in (34) can be used to show that for any fixed $\bar{\lambda}$ there exist arbitrarily large constant parameters a, b verifying

$$\frac{1}{n} \;<\; 2\frac{a}{b}\bar{\lambda} \;<\; \frac{2}{n} - \frac{2}{k_c n} \tag{35}$$

$$b\delta \;>\; \frac{2\left(k_c \frac{n^3}{\delta} + 1\right)\bar{\lambda}^2}{2\frac{a}{b}\bar{\lambda} - \frac{1}{n}} \tag{36}$$

with $\delta = \delta_c$ and $k_c > 2$, such that for all $t \geq 0$

$$P_c \;>\; 0 \tag{37}$$

$$P_c F(t) + F^\top(t) P_c + 2\bar{\lambda} P_c \;<\; 0\,. \tag{38}$$

First we prove the inequality in (37). Let $\eta = [\eta_1^\top \;\; \eta_2^\top]^\top$ with $\eta_1, \eta_2 \in \mathbb{R}^{n-1}$. Then, we have

$$\begin{aligned} \eta^\top P_c \eta \;&=\; \eta_1^\top \eta_1 \;-\; \frac{\delta_c}{\bar{\lambda}n^2}\eta_1^\top QC\eta_2 \;+\; \frac{a\delta_c}{2b\bar{\lambda}n^2}\eta_2^\top \eta_2 \\ &\geq\; \|\eta_1\|^2 \;+\; \frac{a\delta_c}{2b\bar{\lambda}n^2}\|\eta_2\|^2 \;-\; \frac{\delta_c}{\bar{\lambda}n^2}\|QC\|\,\|\eta_1\|\,\|\eta_2\| \\ &=\; \begin{bmatrix} \|\eta_1\| & \|\eta_2\| \end{bmatrix} \begin{bmatrix} 1 & -\frac{\delta_c}{2\bar{\lambda}n^2}\|QC\| \\ -\frac{\delta_c}{2\bar{\lambda}n^2}\|QC\| & \frac{a\delta_c}{2b\bar{\lambda}n^2} \end{bmatrix} \begin{bmatrix} \|\eta_1\| \\ \|\eta_2\| \end{bmatrix} \end{aligned}$$

and, noting that $\|QC\| = 1$, it is easy to verify that $P_c > 0$ if the following condition holds

$$2\frac{a}{b}\bar{\lambda} - \frac{\delta_c}{n^2} \;>\; 0\,.$$

Since $\delta_c \leq n$, the design constraint in (35) ensures that the inequality above is satisfied.

Similarly, we can prove the inequality in (38). From the dynamics in (27) and the definition of P_c in (33) it follows that

$$-\left(P_cF(t)+F^\top(t)P_c+2\bar\lambda P_c\right) \;=\; \begin{bmatrix} 2a\bar L(t)-\frac{b\delta_c}{2\bar\lambda n^2}\left(\bar L(t)QCC^\top Q^\top+QCC^\top Q^\top\bar L(t)\right)-2\bar\lambda\mathbb{I}_{n-1} & -\left(1-\frac{\delta_c}{n^2}\right)QC \\ -\left(1-\frac{\delta_c}{n^2}\right)C^\top Q^\top & \frac{\delta_c}{\bar\lambda n^2}C^\top Q^\top QC-\frac{a\delta_c}{bn^2}\mathbb{I}_{n-1}\end{bmatrix}.$$

Consider now a vector $\eta=[\eta_1^\top\;\eta_2^\top]^\top$ with $\eta_1,\eta_2\in\mathbb{R}^{n-1}$. Then, we can write

$$\begin{aligned}-\eta^\top\left(P_cF(t)+F^\top(t)P_c+2\bar\lambda P_c\right)\eta \;&=\; \eta_1^\top\left(2a\bar L(t)-\frac{b\delta_c}{2\bar\lambda n^2}\left(\bar L(t)QCC^\top Q^\top+QCC^\top Q^\top\bar L(t)\right)-2\bar\lambda\mathbb{I}_{n-1}\right)\eta_1\\ &\quad+\;\eta_2^\top\left(\frac{\delta_c}{\bar\lambda n^2}C^\top Q^\top QC-\frac{a\delta_c}{bn^2}\mathbb{I}_{n-1}\right)\eta_2\;-\;2\left(1-\frac{\delta_c}{n^2}\right)\eta_1^\top QC\eta_2\,.\end{aligned}$$

Since $\|QC\|=1$, $\lambda_{\min}(C^\top Q^\top QC)=\frac{1}{n}$, and $\lambda_{\max}(\bar L(t))\le n$, it follows from the connectivity condition in (34) that

$$\begin{aligned}-\eta^\top\left(P_cF(t)+F^\top(t)P_c+2\bar\lambda P_c\right)\eta \;&\ge\; \left(2a\delta_c-\frac{b\delta_c}{\bar\lambda n}-2\bar\lambda\right)\|\eta_1\|^2\;+\;\left(\frac{1}{n}\frac{\delta_c}{\bar\lambda n^2}-\frac{a\delta_c}{bn^2}\right)\|\eta_2\|^2\\ &\quad-\;2\left(1-\frac{\delta_c}{n^2}\right)\|\eta_1\|\,\|\eta_2\|\\ &=\; \begin{bmatrix}\|\eta_1\| & \|\eta_2\|\end{bmatrix}\begin{bmatrix}2a\delta_c-\frac{b\delta_c}{\bar\lambda n}-2\bar\lambda & -\left(1-\frac{\delta_c}{n^2}\right)\\ -\left(1-\frac{\delta_c}{n^2}\right) & \frac{1}{n}\frac{\delta_c}{\bar\lambda n^2}-\frac{a\delta_c}{bn^2}\end{bmatrix}\begin{bmatrix}\|\eta_1\|\\ \|\eta_2\|\end{bmatrix},\end{aligned}$$

while the design constraints in (35) and (36) guarantee that the above matrix is positive definite. In fact, we note first that the first principal minor of this matrix can be rewritten as

$$2a\delta_c-\frac{b\delta_c}{\bar\lambda n}-2\bar\lambda \;=\; \frac{b\delta_c}{\bar\lambda}\left(2\frac{a}{b}\bar\lambda-\frac{1}{n}\right)-2\bar\lambda$$

and thus the design constraints in (35) and (36) ensure

$$\frac{b\delta_c}{\bar\lambda}\left(2\frac{a}{b}\bar\lambda-\frac{1}{n}\right)-2\bar\lambda \;>\; 0\,.$$

Next, we show that the determinant of the matrix is positive

$$\begin{aligned}\det\left(\begin{bmatrix}2a\delta_c-\frac{b\delta_c}{\bar\lambda n}-2\bar\lambda & -\left(1-\frac{\delta_c}{n^2}\right)\\ -\left(1-\frac{\delta_c}{n^2}\right) & \frac{1}{n}\frac{\delta_c}{\bar\lambda n^2}-\frac{a\delta_c}{bn^2}\end{bmatrix}\right) \;&=\; \left(2a\delta_c-\frac{b\delta_c}{\bar\lambda n}-2\bar\lambda\right)\left(\frac{1}{n}\frac{\delta_c}{\bar\lambda n^2}-\frac{a\delta_c}{bn^2}\right)-\left(1-\frac{\delta_c}{n^2}\right)^2\\ &\ge\; \bar\lambda\left(\frac{b\delta_c}{\bar\lambda^2}\left(2\frac{a}{b}\bar\lambda-\frac{1}{n}\right)-2\right)\left(\frac{2}{n}-2\frac{a}{b}\bar\lambda\right)\frac{\delta_c}{2\bar\lambda n^2}-1\\ &\ge\; \bar\lambda\frac{kn^3}{\delta_c}\left(\frac{2}{n}-2\frac{a}{b}\bar\lambda\right)\frac{\delta_c}{\bar\lambda n^2}-1\\ &=\; kn\left(\frac{2}{n}-2\frac{a}{b}\bar\lambda\right)-1\\ &>\; 2kn\frac{1}{kn}-1\;>\;0\,,\end{aligned}$$

and therefore we can conclude that

$$P_c F(t) + F^\top(t) P_c + 2\bar{\lambda} P_c \quad < \quad 0\,.$$

Hence, using the Lyapunov function candidate in (32), it follows that

$$\begin{aligned} \dot{V}_c(t) &= \zeta^\top(t)(P_c F(t) + F^\top(t) P_c)\zeta(t) \\ &\leq -2\bar{\lambda} V_c(t) \end{aligned}$$

and consequently the system (31) is globally uniformly exponentially stable. We conclude that the forced system (27) is ISS because it is a linear system, $L(t)$ is bounded and the homogeneous equation is exponentially stable (see Ref. [26]), and thus (28) holds.

To prove inequalities (29) and (30), we introduce the *disagreement vector* $\varrho(t) = \Pi l'(t)$ and use the facts that

$$l'_i(t) - l'_j(t) = \varrho_i(t) - \varrho_j(t) \quad i = 1, \ldots, n;\ j = 1, \ldots, n \tag{39}$$

$$\|\varrho(t)\| = \|\zeta_1(t)\| \tag{40}$$

$$\zeta_{2_i}(t) = \chi_{I_i}(t) - \frac{v_{d_1}}{l_{f_1}} \quad i = 1, \ldots, n-1\,. \tag{41}$$

It follows from the relations (39)–(40) that

$$\left|l'_i(t) - l'_j(t)\right| = |\varrho_i(t) - \varrho_j(t)| \leq |\varrho_i(t)| + |\varrho_j(t)| \leq 2\|\varrho(t)\| = 2\|\zeta_1(t)\|\,,$$

and thus equation (28) leads to (29) with $k_3 = 2k_2$.

On the other hand, from (24), (26), and (41) one obtains

$$\begin{aligned} \dot{l}'_1(t) - \frac{v_{d_1}}{l_{f_1}} &= -a \sum_{j \in J_1} (l'_1(t) - l'_j(t)) + \varphi_1(t) \\ \dot{l}'_i(t) - \frac{v_{d_1}}{l_{f_1}} &= -a \sum_{j \in J_i} (l'_i(t) - l'_j(t)) + \zeta_{2_{i-1}} + \varphi_i(t), \quad i = 2, \ldots, n\,, \end{aligned}$$

which, along with (28) and $|\varphi_i(t)| \leq |e_{v_i}(t)|/l_{fi}$, lead to the bound in (30) with $k_4 = (2a\,(n-1)+1)\,k_2 + \frac{1}{l_{f_i}}$. □

Remark 2 *We also note that the design constraint in* (36) *depends upon the lower bound on the second smallest eigenvalue of the Laplacian $L(t)$, which is not known a priori. However, it is well known from algebraic graph theory that the following bound holds*

$$\lambda_2\left(L(t)\right) \geq 2e\left(1 - \cos\left(\frac{\pi}{n}\right)\right)\,,$$

where e is the edge-connectivity of the graph and can be related to the QoS of the network. Then, the parameters a and b can be chosen using this lower bound if a tighter bound is not known a priori.

Next, we consider the case where the communication graph $\Gamma(t)$ may be disconnected during some interval of time or may even fail to be connected at any instant of time; however, we assume that the connectivity of the graph satisfies the following less restrictive persistency of excitation (PE)-like condition

$$\frac{1}{T}\int_t^{t+T} \bar{L}(\tau)d\tau \geq \bar{\mu}\,\mathbb{I}_{n-1}, \quad \forall t \geq 0 \tag{42}$$

for some $T, \bar{\mu} > 0$.

Lemma 3 *Consider the coordination system* (27) *and suppose that the Laplacian of the graph that models the communication topology satisfies the PE condition* (42) *for some* $\bar{\mu}$ *and sufficiently small time* T*. Then, for any given* $\bar{\lambda} > 0$*, there exist sufficiently large coordinated control gains* a, b *such that the system* (27) *is ISS with respect to* $e_v(t)$*, and the normalized lengths* $l_i'(t)$ *and path-length rates* $\dot{l}_i'(t)$ *satisfy* (29) *and* (30)*, respectively.*

Proof. A proof for this lemma can be found in the Appendix. □

Remark 3 *The PE condition* (42) *only requires the graph be connected in an integral sense, not pointwise in time. Similar type of conditions for other coordination laws can be found in e.g. Ref. [27] and Ref. [28] .*

5.0 $\mathcal{L}_1$ ADAPTIVE AUGMENTATION OF COMMERCIAL AUTOPILOTS

So far, both the path following and time-critical coordination strategies were based on vehicle kinematics only (outer-loop control). In this set-up, the pitch and yaw rate inputs $q_c(t)$ and $r_c(t)$ were selected so as to meet the path following objectives, while the speed $v_c(t)$ was computed to achieve coordination. It is now necessary to bring the UAV dynamics into play. To this effect, the above variables must be viewed as commands to be tracked by appropriately designed inner-loop control systems. At this point, a key constraint is included: the inner-loop control systems should build naturally on existent autopilots. Since commercial autopilots are normally designed to track simple way-point commands, we modify the pitch and yaw rates, as well as the speed commands computed before by including an $\mathcal{L}_1$ adaptive loop to ensure that the closed-loop UAV with the autopilot tracks the commands $v_c(t)$, $q_c(t)$, and $r_c(t)$ generated by the time-coordination algorithm and the path following algorithm. The main benefit of the $\mathcal{L}_1$ adaptive controller is its ability of fast and robust adaptation, which leads to desired transient and steady-state performance for the system's both input and output signals simultaneously, in addition to guaranteed gain and time-delay margins. Moreover, analytically computable performance bounds can be derived for the system output as compared to the response of a desired model, which is designed to meet the desired specifications[29–31].

First, we consider the system $\mathcal{G}_p$, which models the closed-loop system of the UAV with the autopilot:

$$\mathcal{G}_p: \quad y(s) \quad = \quad G_p(s)(u(s) + z(s)),$$

where $G_p(s)$ is an unknown strictly proper matrix transfer function, $y(s)$ and $u(s)$ are the Laplace transforms of $y(t)$ and $u(t)$ respectively, and $z(s)$ is the Laplace transform of $z(t)$, which models unknown bounded time-varying disturbances. The system $\mathcal{G}_p$ has the input $u(t) = [v_{ad}(t)\ q_{ad}(t)\ r_{ad}(t)]^\top$ issued from the $\mathcal{L}_1$ adaptive augmentation and output $y(t) = [v(t)\ q(t)\ r(t)]^\top$.

In this paper, $G_p(s)$ is assumed to have the (decoupled) form

$$\mathcal{G}_p \quad : \quad \begin{cases} v(s) = G_v(s)\,(v_{ad}(s) + z_v(s)) \\ q(s) = G_q(s)\,(q_{ad}(s) + z_q(s)) \\ r(s) = G_r(s)\,(r_{ad}(s) + z_r(s)) \end{cases} \tag{43}$$

where $G_v(s)$, $G_q(s)$, $G_r(s)$ are unknown strictly proper and stable transfer functions, and $z_v(s)$, $z_q(s)$, $z_r(s)$ represent the Laplace transformations of the time-varying disturbance signals $z_v(t)$, $z_q(t)$ and $z_r(t)$, respectively. We note that the autopilot is designed to ensure that $y(t)$ tracks any smooth $u(t)$. We further assume that the time-varying disturbances are bounded functions of time with uniformly bounded derivatives:

$$\begin{aligned} |z_v(t)| &\le L_{v0}\,, & |\dot{z}_v(t)| &\le L_{v1} \\ |z_q(t)| &\le L_{q0}\,, & |\dot{z}_q(t)| &\le L_{q1} \\ |z_r(t)| &\le L_{r0}\,, & |\dot{z}_r(t)| &\le L_{r1} \end{aligned}$$

where L_{v0}, L_{v1}, L_{q0}, L_{q1}, L_{r0}, and L_{r1} are some conservative known bounds.

We note that only very limited knowledge of the autopilot is assumed at this point. We do not assume knowledge of the state dimension of the unknown transfer functions $G_v(s)$, $G_q(s)$ and $G_r(s)$. We only assume that these are strictly proper and stable transfer functions. This will make the resulting inner-outer control systems applicable to a wide range of aircraft. We nevertheless notice that the bandwidth of the control channel of the closed-loop UAV with the autopilot is very limited, and the model (43) is valid only for low-frequency approximation of $\mathcal{G}_p$.

Next, since $q_c(t)$ and $r_c(t)$ defined in (16)-(17) stabilize the subsystem $\mathcal{G}_e$, and $v_c(t)$ in (23) (with the coordination control algorithm (24)-(25)) leads to coordination in time, the control objective for the subsystem $\mathcal{G}_p$ is reduced to designing an adaptive output feedback controller $u(t) = [v_{ad}(t)\; q_{ad}(t)\; r_{ad}(t)]^\top$ such that the output $y(t) = [v(t)\; q(t)\; r(t)]^\top$ tracks the reference input $y_c(t) = [v_c(t)\; q_c(t)\; r_c(t)]^\top$ following desired reference models $M_v(s)$, $M_q(s)$, and $M_r(s)$, i.e.

$$\begin{aligned} v(s) &\approx M_v(s)v_c(s) \\ q(s) &\approx M_q(s)q_c(s) \\ r(s) &\approx M_r(s)r_c(s)\,, \end{aligned}$$

where $M_v(s)$, $M_q(s)$, and $M_r(s)$ are designed to meet the desired specifications. In this paper, for simplicity, we consider a first order system[2], by setting

$$M_\bullet(s) = \frac{m_\bullet}{s+m_\bullet}\,, \qquad m_\bullet > 0\,.$$

Finally, we notice that the $\mathcal{L}_1$ adaptive augmentation presented in this section is what allows us to account for the UAV dynamics.

In the following sections, we present the $\mathcal{L}_1$ adaptive augmentation architecture for the inner-loop (see Figure 5), and state a computable uniform performance bound for the tracking error between the output of the adaptive closed-loop system and the reference input signal. We refer to Ref.[24] for a detailed derivation and discussion of this bound. Since the systems in (43) have the same structure, we will define the $\mathcal{L}_1$ adaptive control architecture only for the system $G_q(s)$. The same analysis can be applied to the systems $G_v(s)$ and $G_r(s)$. The stability of the cascaded coordinated path following closed-loop system with the $\mathcal{L}_1$ adaptive augmentation will be proven in Sections 6.0 and 7.0.

5.1 $\mathcal{L}_1$ Adaptive Output Feedback Controller

We notice that the system

$$q(s) = G_q(s)\,(q_{ad}(s) + z_q(s)) \tag{44}$$

can be rewritten in terms of the desired system behavior, defined by $M_q(s)$, as

$$q(s) = M_q(s)\,(q_{ad}(s) + \sigma_q(s))\,, \tag{45}$$

where the uncertainties due to $G_q(s)$ and $z_q(s)$ are lumped in the signal $\sigma_q(s)$, which is defined as

$$\sigma_q(s) = \frac{(G_q(s) - M_q(s))\,q_{ad}(s) + G_q(s)z_q(s)}{M_q(s)}\,. \tag{46}$$

[2]This choice of the desired reference system $M_\bullet(s)$ might represent a limitation on the achievable performance of the adaptive closed-loop system. The choice of a different desired reference system can be explored using the theory developed in Ref. [32], where an extension of the $\mathcal{L}_1$ adaptive output-feedback controller for arbitrary desired reference model is presented.

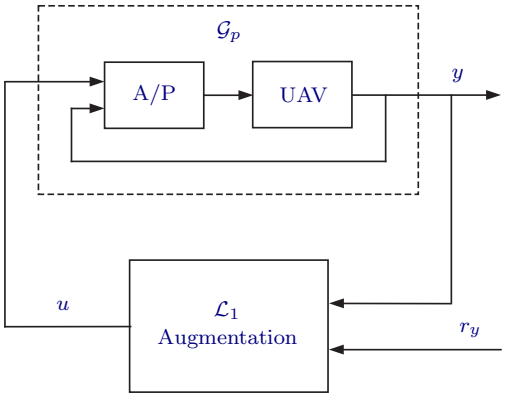

Figure 5: Inner loop structure with the $\mathcal{L}_1$ adaptive augmentation

The philosophy of the $\mathcal{L}_1$ adaptive output feedback controller is to obtain an estimate of the unknown signal $\sigma_q(t)$, and define a *control signal* which compensates for these uncertainties within the bandwidth of a low-pass filter $C(s)$ introduced in the feedback loop. This filter guarantees that the $\mathcal{L}_1$ adaptive controller stays in the low-frequency range even in the presence of high adaptive gains and large reference inputs. The choice of $C(s)$ defines the trade-off between performance and robustness [31]. *Adaptation* is based on the projection operator, ensuring boundedness of the adaptive parameters by definition [33], and uses the output of a *state predictor* to update the estimate of $\sigma_q(t)$. This state predictor is defined to have the same structure of the open-loop system (45), using the estimate of $\sigma_q(t)$ instead of $\sigma_q(t)$ itself, which is unknown. The $\mathcal{L}_1$ adaptive control architecture for the pitch-rate channel is represented in Figure 6 and its elements are introduced below.

State Predictor: We consider the state predictor

$$\dot{\hat{q}}(t) = -m_q \hat{q}(t) + m_q \left(q_{ad}(t) + \hat{\sigma}_q(t)\right), \;\; \hat{q}(0) = q(0), \tag{47}$$

where the adaptive estimate $\hat{\sigma}_q(t)$ is governed by the following adaptation law.

Adaptive Law: The adaptation of $\hat{\sigma}_q(t)$ is defined as

$$\dot{\hat{\sigma}}_q(t) = \Gamma_c \mathrm{Proj}(\hat{\sigma}_q(t), -\tilde{q}(t)), \; \hat{\sigma}_q(0) = 0, \tag{48}$$

where $\tilde{q}(t) = \hat{q}(t) - q(t)$ is the error signal between the state predictor in (47) and the output of the system in (44), $\Gamma_c \in \mathbb{R}^+$ is the adaptation rate subject to a computable lower bound, and Proj denotes the projection operator.

Control Law: The control signal is generated by

$$q_{ad}(s) \;\; = \;\; C_q(s) \left(r_q(s) - \hat{\sigma}_q(s)\right), \tag{49}$$

where $r_q(t)$ is a bounded reference input signal with bounded derivative, and $C_q(s)$ is a strictly proper low-pass filter with $C_q(0) = 1$. In this paper, we consider the simplest choice of a first order filter

$$C_q(s) \;\; = \;\; \frac{\omega_q}{s + \omega_q}, \qquad \omega_q > 0.$$

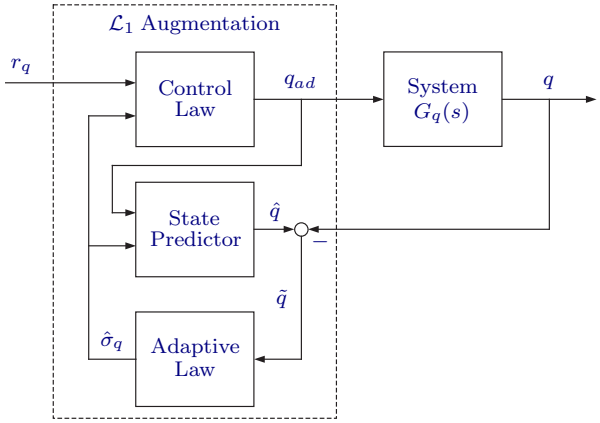

Figure 6: $\mathcal{L}_1$ adaptive augmentation loop for pitch rate control

The complete $\mathcal{L}_1$ adaptive output feedback controller consists of (47), (48) and (49), with $M_q(s)$ and $C_q(s)$ ensuring stability of[3]

$$H(s) \quad = \quad \frac{G_q(s)M_q(s)}{C_q(s)G_q(s) + (1 - C_q(s))M_q(s)}\,. \tag{50}$$

5.2 Analysis of the $\mathcal{L}_1$ Adaptive Controller

In this section we discuss the stability of the closed-loop adaptive system and the performance bound for system's output with respect to the reference command. We avail ourselves of previous work on $\mathcal{L}_1$ augmentation and its application to path following [24, 34] .

Lemma 4 *Let $r_q(t)$ be a bounded reference command with bounded derivative. Given the $\mathcal{L}_1$ adaptive controller defined via (47), (48) and (49) subject to* (50)*, if the adaptation gain Γ_c and the projection bounds are appropriately chosen*[4] *and, moreover, the initial conditions satisfy*

$$|q(0) - r_q(0)| \quad \leq \quad \frac{\gamma_{\dot{r}_q}}{m_q}\,,$$

where $\gamma_{\dot{r}_q}$ is the bound on the derivative of $r_q(t)$, then we have

$$\|q - r_q\|_{\mathcal{L}_\infty} \quad \leq \quad \gamma_\theta \tag{51}$$

where $\gamma_\theta = \gamma_q + \bar{\gamma}_q + \frac{\gamma_{\dot{r}_q}}{m_q}$ and, moreover, $\lim_{\Gamma_c \to \infty} \left(\gamma_q + \lim_{\omega \to \infty} \bar{\gamma}_q\right) = 0$.

[3]This stability condition is a simplified version of the original condition derived in Ref.[34] , where the problem formulation includes output dependent disturbance signals $z(t) = f(t, y(t))$.

[4]See Ref.[24] for a detailed discussion and derivation of the design constraints on the adaptation gain Γ_c, the bandwidth of the low-pass filter ω_q, and the bandwidth of the state-predictor m_q.

Proof. The proof of this Lemma can be found in Ref.[24] . □

Similarly, if we implement the $\mathcal{L}_1$ adaptive controller for the systems

$$\begin{aligned} v(s) &= G_v(s)\left(v_{ad}(s) + z_v(s)\right) \\ r(s) &= G_r(s)\left(r_{ad}(s) + z_r(s)\right) \end{aligned}$$

subject to

$$\begin{aligned} |v(0) - v_c(0)| &\leq \frac{\|\dot{v}_c\|_{\mathcal{L}_\infty}}{m_v}, \\ |r(0) - r_c(0)| &\leq \frac{\|\dot{r}_c\|_{\mathcal{L}_\infty}}{m_r}, \end{aligned}$$

we can derive

$$\|v - v_c\|_{\mathcal{L}_\infty} \leq \gamma_v \tag{52}$$

$$\|r - r_c\|_{\mathcal{L}_\infty} \leq \gamma_\psi \tag{53}$$

with $\gamma_v > 0$ and $\gamma_\psi > 0$ being constants similar to γ_θ. We note that γ_v, γ_θ, and γ_ψ can be rendered arbitrarily small by increasing the adaptation gain Γ_c, the bandwidth of the low-pass filters $\omega_\bullet$, and the bandwidth of the state predictors $m_\bullet$.

Remark 4 *We note that the derivation of the performance bounds with the $\mathcal{L}_1$ adaptive augmentation assumes bounded reference commands with bounded derivatives, and thus before using these performance bounds one should make sure that these conditions are satisfied.*

6.0 PATH FOLLOWING WITH $\mathcal{L}_1$ ADAPTIVE AUGMENTATION

At this point, we discuss the stability of the path following closed-loop system with the $\mathcal{L}_1$ augmentation for a single UAV (see Figure 7). First, we need to show that the outer-loop path following commands $q_c(t)$ and $r_c(t)$ and their derivatives $\dot{q}_c(t)$ and $\dot{r}_c(t)$ are bounded, which in turn allows us to prove that the original domain of attraction for the kinematic error equations given in (18) can be retained with the $\mathcal{L}_1$ augmentation.

Lemma 5 *If $x(t) \in \bar{\Omega}$ for all $t \in [0, \tau]$, where $\bar{\Omega}$ is the closure of the set Ω, which was defined in* (18)*, and the UAV speed $v(t)$ is upper bounded (that is, $v(t) \leq v_{\max}$), then, for sufficiently large Γ_c, and control parameters $\omega_\bullet$ and $m_\bullet$, there exist positive constants γ_{q_c}, $\gamma_{\dot{q}_c}$, γ_{r_c}, and $\gamma_{\dot{r}_c}$ such that the outer-loop path following commands $q_c(t)$ and $r_c(t)$ and their derivatives $\dot{q}_c(t)$ and $\dot{r}_c(t)$ are bounded as*

$$\begin{aligned} \|q_{c\tau}\|_{\mathcal{L}_\infty} &\leq \gamma_{q_c}, & \|\dot{q}_{c\tau}\|_{\mathcal{L}_\infty} &\leq \gamma_{\dot{q}_c} \\ \|r_{c\tau}\|_{\mathcal{L}_\infty} &\leq \gamma_{r_c}, & \|\dot{r}_{c\tau}\|_{\mathcal{L}_\infty} &\leq \gamma_{\dot{r}_c}. \end{aligned} \tag{54}$$

Proof. The proof of this Lemma can be found in Ref.[24]. □

Next, we define $u_\theta(t)$ and $u_\psi(t)$ as

$$\begin{bmatrix} u_\theta(t) \\ u_\psi(t) \end{bmatrix} = D\left(t, \theta_e \psi_e\right) + T\left(t, \theta_e\right) \begin{bmatrix} q(t) \\ r(t) \end{bmatrix}, \tag{55}$$

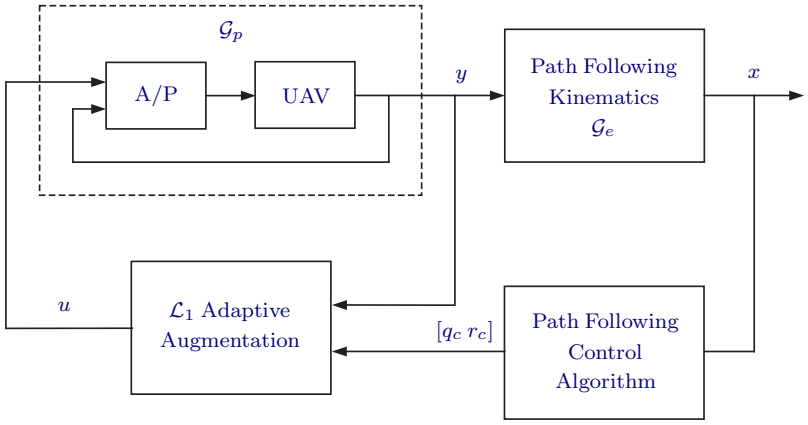

Figure 7: Path following closed-loop system for a single UAV with $\mathcal{L}_1$ adaptive augmentation

and therefore, from (9), one gets

$$\dot{\theta}_e(t) \;=\; u_\theta(t) \qquad \text{and} \qquad \dot{\psi}_e(t) \;=\; u_\psi(t)\,.$$

Then, it follows from (16) and (55) that

$$\begin{bmatrix} u_\theta(t) - u_{\theta_c}(t) \\ u_\psi(t) - u_{\psi_c}(t) \end{bmatrix} \;=\; T\,(t,\theta_e) \begin{bmatrix} q(t) - q_c(t) \\ r(t) - r_c(t) \end{bmatrix}. \tag{56}$$

Furthermore, we define γ_{u_θ} and γ_{u_ψ} as

$$\gamma_{u_\theta} \;=\; \sqrt{\gamma_\theta^2 + \gamma_\psi^2} \qquad \text{and} \qquad \gamma_{u_\psi} \;=\; \frac{1}{\cos\nu_1}\sqrt{\gamma_\theta^2 + \gamma_\psi^2}\,, \tag{57}$$

with γ_θ and γ_ψ being the bounds in (51) and (53) for $r_q(t) \equiv q_c(t)$ and $r_r(t) \equiv r_c(t)$.

Theorem 1 *Let $d = \sqrt{cc_1}$, where c and c_1 were introduced in (14), and let the progression of the point P along the path be governed by (15). For any smooth $v(t)$, verifying (13), if*

1. *the initial condition for the path following state vector satisfies*

$$x(0) \in \Omega\,;$$

2. *the initial conditions for the pitch and yaw rates are bounded as*

$$\begin{aligned} |q(0) - q_c(0)| \;&\leq\; \frac{\gamma_{\dot{q}_c}}{m_q} \\ |r(0) - r_c(0)| \;&\leq\; \frac{\gamma_{\dot{r}_c}}{m_r}\,; \end{aligned}$$

3. *and in addition, the adaptation gain Γ_c is sufficiently high, and the design of $\omega_\bullet$ and $m_\bullet$ is such that*

$$\gamma_{u_\theta} + \gamma_{u_\psi} \;\leq\; \frac{\sqrt{cc_2}}{2}\,\frac{\lambda_{\min}(\bar{Q}_p)}{\lambda_{\max}(P_p)}\,; \tag{58}$$

then $x(t) \in \Omega$ for all $t \geq 0$, and the path following closed-loop cascaded system is ultimately bounded with the bounds given in (20).

Proof. The proof of this Theorem can be found in Ref.[24] . □

Remark 5 *We notice that this approach is different from common backstepping-type analysis for cascaded systems. The advantage of the above structure for the feedback design is that it retains the properties of the autopilot, which is designed to stabilize the inner-loop. As a result, it leads to ultimate boundedness instead of asymptotic stability. From a practical point of view, the procedure adopted for inner/outer loop control system design is quite versatile in that it adapts itself to the particular autopilot installed on-board the UAV.*

7.0 COMBINED PATH FOLLOWING AND TIME-CRITICAL COORDINATION WITH $\mathcal{L}_1$ ADAPTIVE AUGMENTATION

This section addresses the stability properties of the combined coordination/path following systems and the inner-loop with $\mathcal{L}_1$ adaptive augmentation. The complete coordinated path following closed-loop system for a single UAV is presented in Figure 8. The main result is stated in Theorem 2. First, however, we need to show that the outer-loop reference commands $v_c(t)$, $q_c(t)$, and $r_c(t)$ and their derivatives are bounded.

Lemma 6 *Assume that, for any UAV, the path generation algorithm ensures that there exists a positive constant β_0 such that*

$$0 \;<\; \beta_0 \;<\; \frac{1}{\bar{\bar{k}}_1 l_{f_{\max}}} \left(v_{\max} \cos\nu_1 \cos\nu_2 - v_{d_1} \frac{l_{f_{\max}}}{l_{f_1}} - K_1 d \right) \tag{59}$$

where $\bar{\bar{k}}_1 = (2a(n-1)+1)k_1$, $l_{f_{\max}} = \max_i\{l_{f_1,\ldots,l_{f_n}}\}$, and for some sufficiently small set Ω. Under this assumption, on can define positive constants γ_{v_c}, $\gamma_{\dot{v}_c}$, γ_{q_c}, $\gamma_{\dot{q}_c}$, γ_{r_c}, and $\gamma_{\dot{r}_c}$ such that, if $x(t) \in \bar{\Omega}$ for all $t \in [0,\tau]$, and the initial conditions verify the relations

$$\begin{array}{rclcrcl} |v(0)-v_c(0)| & \leq & \frac{\gamma_{\dot{v}_c}}{m_v}\,, & & |v(t_s)-v_c(t_s^+)| & \leq & \frac{\gamma_{\dot{v}_c}}{m_v} \\ |q(0)-q_c(0)| & \leq & \frac{\gamma_{\dot{q}_c}}{m_q}\,, & & |r(0)-r_c(0)| & \leq & \frac{\gamma_{\dot{r}_c}}{m_r} \\ |v_c(0)| & < & \gamma_{v_c}\,, & & |\dot{v}_c(0)| & < & \gamma_{\dot{v}_c} \\ \|\zeta(0)\| & < & \beta_0\,, & & & & \end{array} \tag{60}$$

where t_s are the times at which the communication topology switches, then the coordination/path following outer-loop commands $v_c(t)$, $q_c(t)$ and $r_c(t)$ and their derivatives $\dot{v}_c(t)$, $\dot{q}_c(t)$ and $\dot{r}_c(t)$ are bounded as

$$\begin{array}{rclcrcl} \|v_{c\tau}\|_{\mathcal{L}_\infty} & \leq & \gamma_{v_c}\,, & & \|\dot{v}_{c\tau}\|_{\mathcal{L}_\infty} & \leq & \gamma_{\dot{v}_c} \\ \|q_{c\tau}\|_{\mathcal{L}_\infty} & \leq & \gamma_{q_c}\,, & & \|\dot{q}_{c\tau}\|_{\mathcal{L}_\infty} & \leq & \gamma_{\dot{q}_c} \\ \|r_{c\tau}\|_{\mathcal{L}_\infty} & \leq & \gamma_{r_c}\,, & & \|\dot{r}_{c\tau}\|_{\mathcal{L}_\infty} & \leq & \gamma_{\dot{r}_c}\,. \end{array} \tag{61}$$

Furthermore, the resulting velocity for the ith UAV verifies the a priori *specified upper bound $v_i(t) \leq v_{\max}$ for all $t \in [0,\tau]$.*

Proof. A proof for this lemma can be found in the Appendix. □

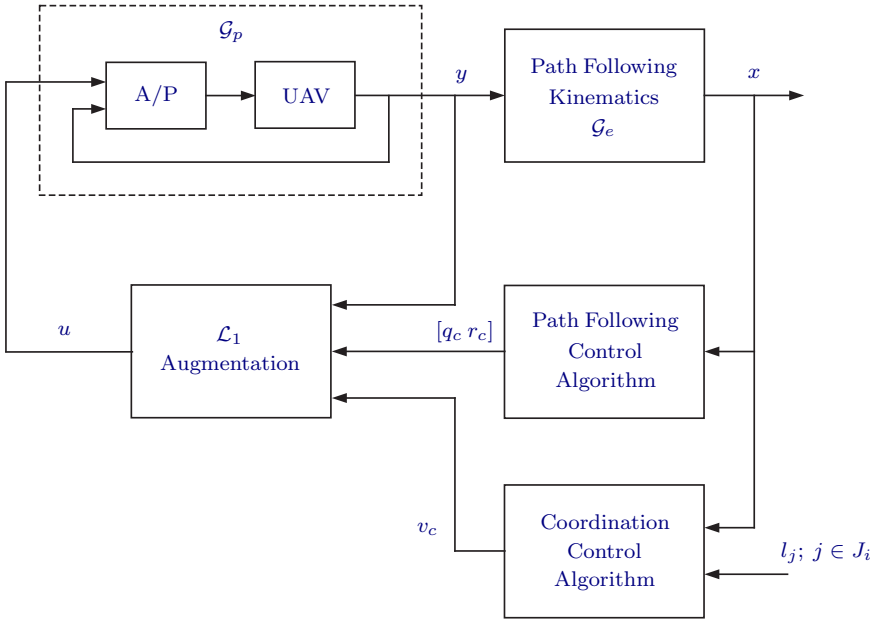

Figure 8: Coordinated path following closed-loop for the ith UAV with $\mathcal{L}_1$ augmentation

Theorem 2 *Consider the combined path following system* (9) *and time-critical coordination system* (27) *under the communication constraints of Lemma 2 or Lemma 3. Assume that the path generation algorithm ensures that there exists a positive constant β_0 such that*

$$0 \;<\; \beta_0 \;<\; \min\left\{ \frac{1}{\bar{\bar{k}}_1 l_{f_{\max}}} \left(v_{\max} \cos\nu_1 \cos\nu_2 - v_{d_1} \frac{l_{f_{\max}}}{l_{f_1}} - K_1 d \right) \;,\; \frac{1}{\bar{\bar{k}}_1 l_{f_{\min}}} \left(v_{d_1} \frac{l_{f_{\min}}}{l_{f_1}} - v_{\min} - K_1 d \right) \right\} \tag{62}$$

where $\bar{\bar{k}}_1$ and $l_{f_{\max}}$ were introduced in Lemma 6, $l_{f_{\min}} = \min\{l_{f_1,\ldots,l_{f_n}}\}$, and for some sufficiently small set Ω. If, for every UAV, we have

1. *the initial condition for the path following state vector satisfies*

$$x_i(0) \in \Omega\,;$$

2. *the initial conditions for the speed, pitch rate, and yaw rate are bounded as*

$$\begin{aligned} |v_i(0) - v_{c_i}(0)| &\leq \tfrac{\gamma_{\dot{v}_c}}{m_v}\,, & |v_i(t_s) - v_{c_i}(t_s^+)| &\leq \tfrac{\gamma_{\dot{v}_c}}{m_v} \\ |q_i(0) - q_{c_i}(0)| &\leq \tfrac{\gamma_{\dot{q}_c}}{m_q}\,, & |r_i(0) - r_{c_i}(0)| &\leq \tfrac{\gamma_{\dot{r}_c}}{m_r} \\ |v_{c_i}(0)| &< \gamma_{v_c}\,, & |\dot{v}_{c_i}(0)| &< \gamma_{\dot{v}_c} \end{aligned} \tag{63}$$

   where γ_{v_c}, $\gamma_{\dot{v}_c}$, $\gamma_{\dot{q}_c}$, and $\gamma_{\dot{r}_c}$ were introduced in (61)*; and*

3. *the initial condition for the coordination state vector satisfies*

$$\|\zeta(0)\| \;<\; \beta_0\,;$$

then, there exist sufficiently large adaptation gain Γ_c and controller parameters $\omega_\bullet$ and $m_\bullet$ such that $x_i(t) \in \Omega$ for all $t \geq 0$ and $i = 1, \ldots, n$, and the complete closed-loop cascaded system is ultimately bounded with the bounds given in (20). Moreover, the coordination error $\zeta(t)$ satisfies

$$\|\zeta(t)\| \quad \leq \quad k_1 \, \|\zeta(0)\| \, \mathrm{e}^{-\bar{\lambda} t} + k_2 \bar{\gamma}_v \, , \tag{64}$$

and the resulting velocity for the ith UAV verifies the a priori *specified bounds $0 < v_{\min} \leq v_i(t) \leq v_{\max}$.*

Proof. Consider the ith UAV. Using the same Lyapunov function candidate $V_p(x)$ as in Lemma 1, it follows that

$$\dot{V}_{p_i} \quad \leq \quad -x_i^\top Q_{p_i} x_i \; + \; \frac{|\theta_{e_i} - \delta_{\theta_i}|}{c_2} \, |u_{\theta_i} - u_{\theta_{ci}}| \; + \; \frac{|\psi_{e_i} - \delta_{\psi_i}|}{c_2} \, |u_{\psi_i} - u_{\psi_{ci}}| \, , \tag{65}$$

where Q_{p_i} was defined in (19), and we have taken into consideration the errors between $u_{\theta_i}(t)$ and $u_{\theta_{ci}}(t)$, and $u_{\psi_i}(t)$ and $u_{\psi_{ci}}(t)$ (or equivalently between $q_i(t)$ and $q_{c_i}(t)$, and $r_i(t)$ and $r_{c_i}(t)$). Next we will show that, under the conditions of the Theorem, Q_{p_i} is positive definite and the terms $|\theta_{e_i} - \delta_{\theta_i}|$, $|u_{\theta_i} - u_{\theta_{ci}}|$, $|\psi_{e_i} - \delta_{\psi_i}|$, and $|u_{\psi_i} - u_{\psi_{ci}}|$ are bounded, and thus the original domain of attraction for the kinematic error equations given in (18) can be retained.

We prove this Theorem by contradiction. Since $x_i(0) \in \Omega$ by assumption, and $V_{p_i}(t)$ is continuous and differentiable, if $x_i(t) \in \Omega \;\; \forall t \geq 0$ is not true, then there exists a time τ such that

$$\begin{aligned} V_{p_i}(t) \quad &< \quad \frac{c}{2} \, , \qquad \forall \, 0 \leq t < \tau \\ V_{p_i}(\tau) \quad &= \quad \frac{c}{2} \, , \end{aligned} \tag{66}$$

which implies

$$\dot{V}_{p_i}(\tau) \quad > \quad 0 \, . \tag{67}$$

First, we show that the speed of the ith UAV verifies $v_i(t) > v_{\min}$ for all $t \in [0, \tau]$, which in turn will help us prove that Q_{p_i} is positive definite. To this aim, we introduce the following notation

$$\epsilon_0 \quad = \quad \min \left\{ \frac{v_{\max} \cos \nu_1 \cos \nu_2 - v_{d_1} \frac{l_{f_{\max}}}{l_{f_1}} - K_1 d - \bar{\bar{k}}_1 \beta_0 l_{f_{\max}}}{\cos \nu_1 \cos \nu_2 \; + \; \bar{\bar{k}}_2 l_{f_{\max}}} \, , \; \frac{v_{d_1} \frac{l_{f_{\min}}}{l_{f_1}} - v_{\min} - K_1 d - \bar{\bar{k}}_1 \beta_0 l_{f_{\min}}}{1 + \bar{\bar{k}}_2 l_{f_{\min}}} \right\} \, ,$$

where $\bar{\bar{k}}_1$ was introduced in Lemma 6 and $\bar{\bar{k}}_2 = (2a(n-1)+1)k_2$. Condition (62) ensure that $\epsilon_0 > 0$. Further, let ϵ be defined as

$$\epsilon \quad < \quad \epsilon_0 \, ,$$

and choose the adaptation gain Γ_c, ω_v, and m_v so that $\bar{\gamma}_v = \max\{\gamma_{v_1}, \ldots, \gamma_{v_n}\}$ verifies the following condition

$$\bar{\gamma}_v \quad < \quad \epsilon \, . \tag{68}$$

Then, it follows from Lemma 6 that the commanded reference signals $v_{c_i}(t)$, $q_{c_i}(t)$, and $r_{c_i}(t)$ and their derivatives $\dot{v}_{c_i}(t)$, $\dot{q}_{c_i}(t)$, and $\dot{r}_{c_i}(t)$ are bounded for all $t \in [0, \tau]$, i.e.

$$\begin{array}{lcllcl} \|v_{c_i \tau}\|_{\mathcal{L}_\infty} & \leq & \gamma_{v_c} \, , & \|\dot{v}_{c_i \tau}\|_{\mathcal{L}_\infty} & \leq & \gamma_{\dot{v}_c} \\ \|q_{c_i \tau}\|_{\mathcal{L}_\infty} & \leq & \gamma_{q_c} \, , & \|\dot{q}_{c_i \tau}\|_{\mathcal{L}_\infty} & \leq & \gamma_{\dot{q}_c} \\ \|r_{c_i \tau}\|_{\mathcal{L}_\infty} & \leq & \gamma_{r_c} \, , & \|\dot{r}_{c_i \tau}\|_{\mathcal{L}_\infty} & \leq & \gamma_{\dot{r}_c} \, , \end{array} \tag{69}$$

and moreover one has

$$v_i(t) \;\leq\; v_{\max}\,, \qquad \forall t \in [0,\tau]\,.$$

Therefore, from this result and the bounds on the initial conditions in (63), one finds that the bounds in (51), (52), and (53) hold with $r_v(t) \equiv v_{c_i}(t)$, $r_q(t) \equiv q_{c_i}(t)$, $r_r(t) \equiv r_{c_i}(t)$, and for any $t \in [0,\tau]$. So we have

$$\left\|(v_i - v_{c_i})_\tau\right\|_{\mathcal{L}_\infty} \;\leq\; \gamma_{v_i} \tag{70}$$
$$\left\|(q_i - q_{c_i})_\tau\right\|_{\mathcal{L}_\infty} \;\leq\; \gamma_{\theta_i} \tag{71}$$
$$\left\|(r_i - r_{c_i})_\tau\right\|_{\mathcal{L}_\infty} \;\leq\; \gamma_{\psi_i}\,. \tag{72}$$

Using (28), similar to (30), it can be shown that

$$u_{\text{coord}_i}(t) \;\geq\; \frac{v_{d_1}}{l_{f_1}} - \bar{\bar{k}}_1 \left\|\zeta(0)\right\| - \bar{\bar{k}}_2 \sup_{t\in[0,\tau]} \left\|e_v(t)\right\|\,. \tag{73}$$

Since at any $t \in [0,\tau]$ the path following error states $x_i(t)$ lie in the compact set $\bar{\Omega}$, then

$$v_{c_i}(t) \;\geq\; u_{coord_i}(t) l_{f_i} - K_1 d\,,$$

and thus,

applying (68), (70), and (73) to the above inequality yields

$$\begin{aligned} v_{c_i}(t) \;&\geq\; v_{d_1}\frac{l_{f_i}}{l_{f_1}} - \bar{\bar{k}}_1 \left\|\zeta(0)\right\| l_{f_i} - \bar{\bar{k}}_2 \bar{\gamma}_v l_{f_i} - K_1 d \\ &>\; v_{d_1}\frac{l_{f_i}}{l_{f_1}} - \bar{\bar{k}}_1 \left\|\zeta(0)\right\| l_{f_i} - \bar{\bar{k}}_2 \epsilon_0 l_{f_i} - K_1 d \\ &>\; \left(\frac{v_{d_1}}{l_{f_1}} - \bar{\bar{k}}_1 \beta_0 - \bar{\bar{k}}_2 \epsilon_0\right) l_{f_{\min}} - K_1 d \\ &\geq\; v_{\min} + \epsilon_0\,. \end{aligned}$$

Finally, since $\|(e_{v_i})_\tau\|_{\mathcal{L}_\infty} \leq \gamma_{v_i}$, it follows that

$$v_i(t) \;\geq\; v_{c_i}(t) - \gamma_{v_i} \;\geq\; v_{c_i}(t) - \bar{\gamma}_v \;>\; v_{\min} + (\epsilon_0 - \bar{\gamma}_v) \;>\; v_{\min}\,,$$

for all $t \in [0,\tau]$. This result, along with the fact that $x_i(t) \in \bar{\Omega}$ for any $t \in [0,\tau]$, leads to

$$\dot{V}_{p_i} \;\leq\; -x_i^\top \bar{Q}_{p_i} x_i \;+\; \frac{|\theta_{e_i} - \delta_{\theta_i}|}{c_2}\left|u_{\theta_i} - u_{\theta_{ci}}\right| \;+\; \frac{|\psi_{e_i} - \delta_{\psi_i}|}{c_2}\left|u_{\psi_i} - u_{\psi_{ci}}\right|\,, \qquad \forall t \in [0,\tau]\,,$$

where $\bar{Q}_{p_i}$ was defined in (21).

Next we show that, under the conditions of the Theorem, the terms $|\theta_{e_i} - \delta_{\theta_i}|$, $|u_{\theta_i} - u_{\theta_{ci}}|$, $|\psi_{e_i} - \delta_{\psi_i}|$, and $|u_{\psi_i} - u_{\psi_{ci}}|$ are bounded. It follows from (56) that

$$\begin{aligned} u_{\theta_i}(t) - u_{\theta_{ci}}(t) \;&=\; \cos\phi_{e_i}(t)\left(q_i(t) - q_{c_i}(t)\right) - \sin\phi_{e_i}(t)\left(r_i(t) - r_{c_i}(t)\right) \\ u_{\psi_i}(t) - u_{\psi_{ci}}(t) \;&=\; \frac{\sin\phi_{e_i}(t)}{\cos\theta_{e_i}(t)}\left(q_i(t) - q_{c_i}(t)\right) + \frac{\cos\phi_{e_i}(t)}{\cos\theta_{e_i}(t)}\left(r_i(t) - r_{c_i}(t)\right)\,, \end{aligned}$$

and hence, from the bounds in (71) and (72), we have

$$\|(u_{\theta_i} - u_{\theta_{ci}})_\tau\|_{\mathcal{L}_\infty} \;\leq\; \gamma_{u_{\theta i}} \qquad \text{and} \qquad \|(u_{\psi_i} - u_{\psi_{ci}})_\tau\|_{\mathcal{L}_\infty} \;\leq\; \gamma_{u_{\psi i}}\,, \tag{74}$$

with $\gamma_{u_{\theta i}}$ and $\gamma_{u_{\psi i}}$ defined in (57). Moreover, it follows from (66) that for any $t \in [0, \tau]$

$$|\theta_{e_i}(t) - \delta_{\theta_i}(t)| \;\leq\; \sqrt{cc_2} \qquad \text{and} \qquad |\psi_{e_i}(t) - \delta_{\psi_i}(t)| \;\leq\; \sqrt{cc_2}\,. \tag{75}$$

Therefore, from Eqs. (65), (74) and (75), one finds

$$\dot{V}_{p_i}(\tau) \;\;\leq\;\; -x_i^\top(\tau)\bar{Q}_{p_i}x_i(\tau) + \sqrt{\frac{c}{c_2}}(\gamma_{u_{\theta i}} + \gamma_{u_{\psi i}})\,.$$

Since

$$x_i^\top(\tau)\bar{Q}_{p_i}x(\tau) \;\;\geq\;\; \frac{\lambda_{\min}(\bar{Q}_{p_i})}{\lambda_{\max}(P_{p_i})}V_{p_i}(\tau)\,,$$

where $\lambda_{\min}(\bar{Q}_{p_i})$ and $\lambda_{\max}(P_{p_i})$ are the minimum and the maximum eigenvalues of $\bar{Q}_{p_i}$ and P_{p_i} respectively, it follows from (66) that

$$x_i^\top(\tau)\bar{Q}_{p_i}x_i(\tau) \;\;\geq\;\; \frac{c}{2}\frac{\lambda_{\min}(\bar{Q}_{p_i})}{\lambda_{\max}(P_{p_i})}\,,$$

and then the design constraint in (58) leads to

$$\dot{V}_{p_i}(\tau) \;\;\leq\;\; 0\,,$$

which contradicts the assumption in (67), and thus $x_i(t) \in \Omega$ holds for all $t \geq 0$ and $i = 1, \ldots, n$. Since (66) leads to (69)-(75) for any time $t \in [0, \tau]$, $x_i(t) \in \Omega$ implies that the bounds in (20) hold for all $t \geq 0$.

Finally, equations (28) and (70) lead to the bound in (64), which concludes the proof. □

8.0 EXPERIMENTAL RESULTS

The complete coordinated path following control system with $\mathcal{L}_1$ adaptive augmentation, shown in Figure 8, was implemented on experimental UAV RASCALs operated by NPS, and thoroughly tested in hardware-in-the-loop (HIL) simulations and flights at Camp Roberts, CA. The HIL and flight test setups [23] are shown in Figure 9. The payload bay of each aircraft was used to house two PC-104 embedded computers assembled in a stack, wireless network link, and the Piccolo autopilot [35] with its dedicated control channel providing 20 Hz update capability. The first PC-104 board (see SBC (RT) in Figure 9) runs developed path following, adaptation and coordination algorithms in real-time while directly communicating with the autopilot (A/P) at 20 Hz over the dedicated serial link. The second PC-104 computer (see SBC (Win) in Figure 9) is equipped with a mesh network card (Motorola WMC6300 Mesh Card) that provides wireless communication to other identically equipped UAVs as well as to the data processing center on the ground. This second computer performs software bridging of onboard wired and external wireless mesh networks. Thus, direct connection with the onboard autopilot efficiently eliminates communication delays between the high-level control algorithm and the autopilot. In turn, an integration of the self-configuring wireless mesh network allows for transparent inter-vehicle communication making it suitable for coordination in time.

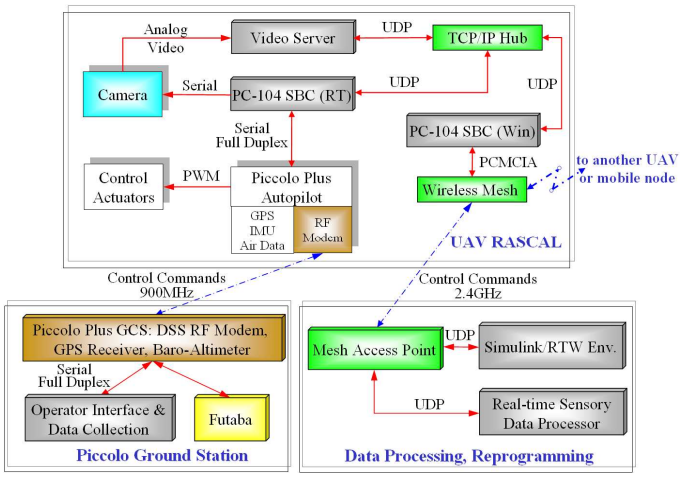

Figure 9: Avionics architecture including two embedded processors and an A/P.

When each UAV is flying in path following mode, the control command, specifying the final conditions (Fin.C.) and initializing the path following algorithm as well as the control system parameters, are initiated from the ground control station to each UAV over a wireless link. Upon receipt of the initialization signal onboard of each vehicle, the UAV states are captured as initial conditions (I.C.). Together with predefined Fin.C., they provide boundary conditions for the path generation algorithm. From that moment on, the UAV tracks the feasible path with the activated path following controller until it arrives to the vicinity of the terminal point. Upon arrival, it can be either automatically stopped, transferring the UAV to the standard A/P control mode, or new terminal conditions can be automatically specified allowing for the experiment to be continued. While in flight, the onboard system continuously logs and transmits UAV telemetry and controller data to the ground, which is essential for safety of the flight, real-time monitoring and tuning of the control system. Based on the presented hardware setup, the developed coordinated path following algorithm has been extensively tested both in HIL simulations and actual flight tests during the years 2007 and 2008.

Figure 10 shows flight test results obtained in February 2007. The objective of these flights was to show the improvement in path following performance that it is obtained with the $\mathcal{L}_1$ adaptive augmentation (Figure 10a). Red trajectories represent the required/commanded flight path, while the blue ones show the actual flight path of the UAV. Figure 10b presents a collective picture of 15 trials obtained during just one flight test. Each trial was used to tune the control law parameters in order to achieve more accurate path following and coordination. For these experiments, the speed of the (virtual) cooperative UAV was simulated to be constant.

Flight test results obtained in February 2008 are shown in Figure 11. They include the 2D projection of the commanded and actual paths, and the path tracking errors $y_F(t)$ and $z_F(t)$. Although the generated commanded path was obviously not feasible (for 25 deg limit of bank angle), the $\mathcal{L}_1$ augmented control system recovers from a 140 m overshoot in the lateral channel in less than 20 s without oscillations, while keeping the path following errors below 15 m for the rest of the 95- seconds-flight. No roll oscillations were observed during that trial.

Figures 12a-12b include results of a HIL test performed in 2007 where two UAVs follow feasible trajectories while using their velocities to coordinate simultaneous arrival at their respective terminal conditions over a fixed communication topology (the UAVs were exchanging information all the time). Figure 12a shows the 2D projection of the desired path and the actual path of each UAV. The normalized coordination states for each UAV are presented in Figure 12b. Both airplanes arrive at the final position at nearly the same time.

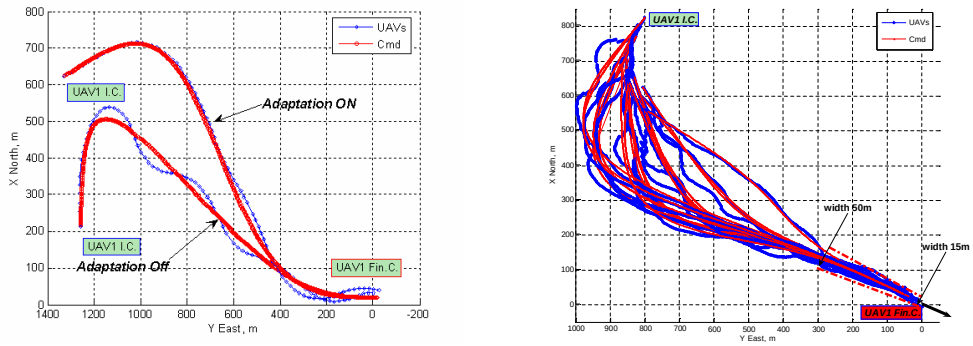

(a) Path tracking (2D projection)

(b) Path tracking – collective picture

Figure 10: FT'07. Path following performance comparison with and without $\mathcal{L}_1$ adaptive augmentation.

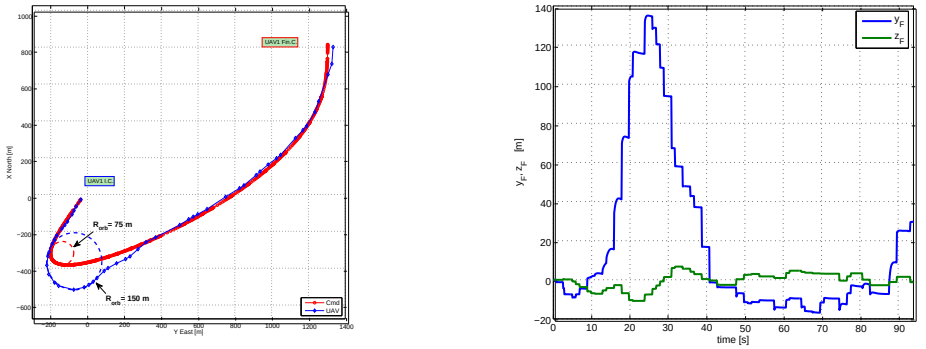

(a) Path tracking (2D projection)

(b) Path following errors $y_F(t)$ and $z_F(t)$

Figure 11: FT'08. Path following performance with $\mathcal{L}_1$ adaptive augmentation.

Finally, Figure 13 illustrates feasibility of the CPF concept for the case of three UAVs using a new more versatile Simulink-based HIL setup (see Ref. [36]). In particular it illustrates (i) the real-time generation of three spatially deconflicted trajectories; (ii) path optimization with an emphasis on the simultaneous arrival and sufficient margin of the arrival time; and (iii) path following and coordination along the assigned trajectories. The number of parameters used to obtain a trajectory for each player included the dimensionless path length, the constant speed profile, and three derivatives of the path at initial (yaw rate) and final (pitch rate and yaw rate) conditions. The hypothetical mission considers exchanging of initial and final conditions by three dynamically different airplanes – they have different masses and engine models. Initially the UAVs are at the colliding course at 500 m from the origin with the bearing separation of 120 deg. The communication architecture assumes instantaneous exchange of relative position of each UAV with its neighbor every 2 seconds in cyclic order, which implies that the graph that captures the underlying communication network topology is not connected at any time (see Figure 13b).

Analysis of the obtained results confirms spatial separation of the trajectories. As one can easily see, in order to maintain the minimum separation distance of 100 m assigned to the path optimizer, the path generation algorithm produces two diving paths and one climbing path. 3D quality of this result is more explicit in Figure 13a. The total path lengths for every path are different, while the corresponding (constant) speed profiles

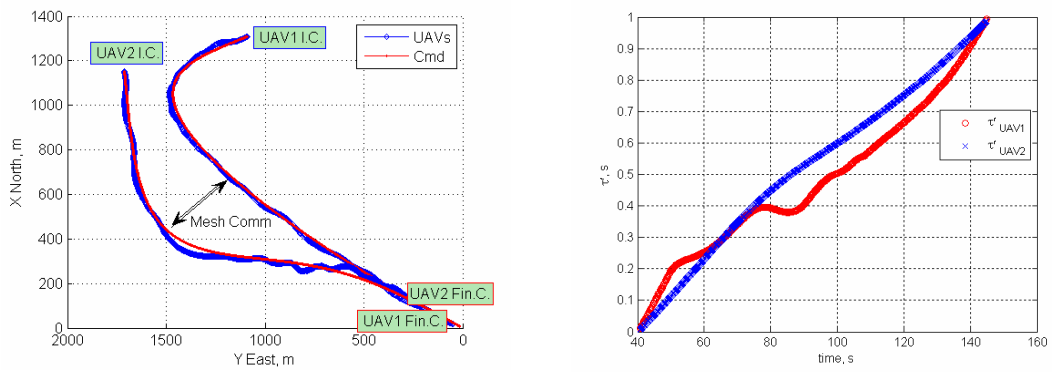

(a) Path tracking (2D projection)

(b) Coordination states for each UAV.

Figure 12: HIL'07. Simultaneous arrival of two UAVs at the same terminal conditions (separated by altitude).

satisfy the limitations on minimum and maximum speed ($15\ \frac{\mathrm{m}}{\mathrm{s}}$ and $30\ \frac{\mathrm{m}}{\mathrm{s}}$, respectively). Although dynamically different, the UAVs track the assigned trajectories and arrive to the final conditions with a time separation of $0.95\ \mathrm{s}$, which is less than the time separation predicted by the optimization algorithm $1.4\ \mathrm{s}$.

The results presented above demonstrate feasibility of the onboard integration of the path following, adaptation and coordination algorithms. During the flight experiments, the required control commands (including the adaptive contribution) never exceeded the limits defined for the UAV in traditional waypoint navigation mode. At the same time, the achieved functionality of the UAV following 3D curves in inertial space has never been available for the airplanes equipped with traditional A/P; the $\mathcal{L}_1$ adaptive augmentation explicitly outperforms the conventional waypoint navigation method. These results provide also a roadmap for further development and onboard implementation of intelligent multi-UAV coordination.

9.0 CONCLUSION

This paper presented a solution to the problem of coordinated path following control of multiple UAVs in the presence of time-varying communication topologies with the objective of meeting desired spatial and/or temporal constraints. As a motivating example, a scenario was considered where a fleet of UAVs must follow spatially deconflicted paths and arrive at their final destinations at identical times. The theoretical framework adopted led to a novel methodology for coordinated motion control that brings together algorithms for path following and vehicle coordination with an inner-outer (that is, kinematic versus dynamic) structure with $\mathcal{L}_1$ adaptation. This is in striking contrast with other algorithms proposed in the literature that yield control laws which are hard to tune and do not exploit the fact that many autonomous vehicles are naturally equipped with local, highly performing dynamic control loops (autopilots).

Central to the development of the control laws derived was the combination of nonlinear path following algorithms, derived at the kinematic level, with an $\mathcal{L}_1$ adaptive output feedback control law that effectively augments an existing autopilot and yields an inner-outer loop control structure with guaranteed performance. The same principle was used at the coordination level, where multiple vehicle coordination laws that generate desired speed profiles for the vehicles in response to data exchanged over a dynamically changing communication are complemented with inner speed control loops that are designed by resorting to $\mathcal{L}_1$ adaptive control techniques. From a theoretical standpoint, the paper offered a complete analysis of the stability properties of the Combined Path Following and Time-Critical Coordination with $\mathcal{L}_1$ Adaptive Augmentation under time-varying

communication constraints. In particular, tools were developed to address explicitly the case where the communication graph that captures the underlying communication network topology may be disconnected during some interval of time or may even fail to be connected at any instant of time. Flight tests and hardware-in-the-loop simulations have shown clearly what steps are required to transition from theory to practice. The results obtained show that the methodology proposed holds considerable promise for coordinated motion control of multiple UAVs.

ACKNOWLEDGMENTS

Research supported in part by projects GREX / CEC-IST (Contract No. 035223), NAV-Control / FCT-PT (PTDC/EEA-ACR/65996/2006), FREESUBNET RTN of the CEC, the FCT-ISR/IST plurianual funding program through the POS_C Program that includes FEDER funds, USSOCOM, ONR under Contract N00014-05-1-0828, AFOSR under Contract No. FA9550-05-1-0157, and ARO under Contract No.W911NF-06-1-0330.

REFERENCES

[1] Kaminer, I., Pascoal, A., Hallberg, E., and Silvestre, C., "Trajectory Tracking for Autonomous Vehicles: An Integrated Approach to Guidance and Control," *AIAA Journal of Guidance, Control, and Dynamics*, Vol. 21, No. 1, 1998.

[2] Kim, Y. and Mesbahi, M., "On Maximizing the Second Smallest Eigenvalue of State-Dependent Graph Laplacian," *IEEE Trans. on Autom. Cont.*, Vol. 51, No. 1, 2006, pp. 116–120.

[3] Tsitsiklis, J. and Athans, M., "Convergence and Asymptotic Agreement in Distributed Decision Problems," *IEEE Transaction on Autom. Cont.*, Vol. 29, No. 1, 1984, pp. 42–50.

[4] Sepulchre, R., Paley, D., and Leonard, N., "Collective Motion and Oscillator Synchronization," *Proc. of Block Island Workshop on Cooperative Control*, Block Island, RI, 2003, pp. 189–205.

[5] Jadbabaie, A., Lin, J., and Morse, A., "Coordination of Groups of Mobile Autonomous Agents using Nearest Neighbor Rules," *IEEE Trans. on Autom. Cont.*, Vol. 48, No. 6, 2003, pp. 988–1001.

[6] Lin, Z., Francis, B., and Maggiore, M., "State Agreement for Coupled Nonlinear Systems with Time-Varying Interaction," *SIAM Journal of Control and Optimization*, 2005, in review.

[7] Egerstedt, M. and Hu, X., "Formation Control with Virtual Leaders and Reduced Communications," *IEEE Trans. on Robotics and Automation*, Vol. 17, No. 6, Dec. 2001, pp. 947–951.

[8] Ghabcheloo, R., Pascoal, A., Silvestre, C., and Kaminer, I., "Coordinated Path Following Control of Multiple Wheeled Robots using Linearization Techniques," *International Journal of Systems Science, Taylor and Francis*, Vol. 37, No. 6, 2006, pp. 399–414.

[9] Fang, L., Antsaklis, P., and Tzimas, A., "Asynchronous Consensus Protocols: Preliminary Results, Simulations and Open Questions," *Proc. of IEEE Conf. on Decision and Control*, Seville, Spain, 2005, pp. 2194–2199.

[10] Mesbahi, M., "On State-Dependent Dynamic Graphs and Their Controllability Properties," *IEEE Trans. on Autom. Cont.*, Vol. 50, No. 3, 2005, pp. 387–392.

[11] Stilwell, D. and Bishop, B., "Platoons of Underwater Vehicles," *IEEE Control Systems Magazine*, Vol. 20, No. 6, Dec. 2000, pp. 45–52.

[12] Stilwell, D., Bollt, E., and Roberson, D., "Sufficient Conditions for Fast Switching Synchronization in Time-Varying Network Topologies," *SIAM Journal of Applied Dynamical Systems*, Vol. 6, No. 1, 2006, pp. 140–156.

[13] Cao, M., Spielman, D., and Morse, A., "A Lower Bound on Convergence of a Distributed Network Consensus Algorithm," *Proc. of IEEE Conf. on Decision & Control*, Seville, Spain, 2005, pp. 2356–2361.

[14] Mesbahi, M. and Hadaegh, F., "Formation Flying Control of Multiple Spacecraft via Graphs, Matrix Inequalities, and Switching," *AIAA Journal of Guidance, Control, and Dynamics*, Vol. 24, No. 2, 2001, pp. 369–377.

[15] Song, Y., Li, Y., and Liao, X., "Orthogonal Transformation Based Robust Adaptive Close Formation Control of Multi-UAVs," *Proc. of American Control Conf.*, Portland, OR, 2005, pp. 2983–2988.

[16] Stipanovic, D., Inalhan, G., Teo, R., and Tomlin, C., "Decentralized Overlapping Control of a Formation of Unmanned Aerial Vehicles," *Automatica*, Vol. 40, No. 1, 2004, pp. 1285–1296.

[17] Ghabcheloo, R., Aguiar, P., Pascoal, A., Silvestre, C., Kaminer, I., and Hespanha, J., "Coordinated Path Following Control of Autonomous Underwater Vehicles in Presence of Communication Failures," *Proc. of IEEE Conf. on Decision and Control*, San Diego, CA, 2006.

[18] Pereira, F. and Sousa, J., "Coordinated Control of Networked Vehicles: An Autonomous Underwater System," *Automation and Remote Control*, Vol. 65, No. 7, 2004, pp. 1037–1045.

[19] Kaminer, I., Yakimenko, O., Dobrokhodov, V., Pascoal, A., Hovakimyan, N., Patel, V. V., Cao, C., and Young, A., "Coordinated Path Following for Time-Critical Missions of Multiple UAVs via $\mathcal{L}_1$ Adaptive Output Feedback Controllers," *AIAA Guidance, Navigation and Control Conference, AIAA 2007-6409, Hilton Head Island, SC*, August 2007.

[20] Yakimenko, O., "Direct Method for Rapid Prototyping of Near-Optimal Aircraft Trajectories," *AIAA Journal of Guidance, Control, & Dynamics*, Vol. 23, No. 5, 2000, pp. 865–875.

[21] Soetanto, D., Lapierre, L., and Pascoal, A., "Adaptive, Non-Singular Path Following, Control of Dynamic Wheeled Robots," *Proc. ICAR*, Coimbra, Portugal, 2003.

[22] A. Micaelli and C. Samson, "Trajectory-Tracking for Unicycle-Type and Two-Steering-Wheels Mobile Robot," Tech. Rep. 2097, INRIA, Sophia-Antipolis, France, 1993.

[23] Kaminer, I., Yakimenko, O., Pascoal, A., and Ghabcheloo, R., "Path Generation, Path Following and Coordinated Control for TimeCritical Missions of Multiple UAVs," *American Control Conference*, June 2006, pp. 4906 – 4913.

[24] Kaminer, I., Pascoal, A., Xargay, E., Cao, C., Hovakimyan, N., and Dobrokhodov, V., "3D Path Following for Small UAVs using Commercial Autopilots augmented by $\mathcal{L}_1$ Adaptive Control," Submitted to *Journal of Guidance, Control and Dynamics*.

[25] Biggs, N., *Algebraic Graph Theory*, Cambridge University Press, 1993.

[26] Khalil, H. K., *Nonlinear Systems*, Third Edition, Prentice Hall, 2002.

[27] Lin, Z., Francis, B., and Maggiore, M., "State Agreement for Continuous-time Coupled Nonlinear Systems," *SIAM Journal of Control and Optimization*, Vol. 46, No. 1, 2007, pp. 288–307.

[28] Arcak, M., "Passivity as a desing tool for group coordination." *IEEE Trans. on Autom. Cont.*, Vol. 52, No. 8, August 2007, pp. 1380–1390.

[29] C. Cao and N. Hovakimyan, "Design and Analysis of a Novel $\mathcal{L}_1$ Adaptive Control Architecture with Guaranteed Transient Performance," *IEEE Transactions on Automatic Control*, Vol. 53, No. 3, 2008, pp. 586–591.

[30] Cao, C. and Hovakimyan, N., "Guaranteed Transient Performance with $\mathcal{L}_1$ Adaptive Controller for Systems with Unknown Time-Varying Parameters and Bounded Disturbances: Part I," *In Proc. of American Control Conference*, New York, NY, July 2007, pp. 3925–3930.

[31] Cao, C. and Hovakimyan, N., "Stability Margins of $\mathcal{L}_1$ Adaptive Controller: Part II," *In Proc. of American Control Conference*, New York, NY, July 2007, pp. 3931–3936.

[32] Cao, C. and Hovakimyan, N., "$\mathcal{L}_1$ Adaptive Output Feedback Controller for Non-Strictly Positive Real Reference Systems with Applications to Aerospace Examples," *AIAA Guidance, Navigation, and Control Conference and Exhibit*, Honolulu, HI, August 2008.

[33] Pomet, J. B. and Praly, L., "Adaptive Nonlinear Regulation: Estimation from the Lyapunov Equation," *IEEE Trans. Autom. Contr.*, Vol. 37(6), June 1992, pp. 729–740.

[34] Cao, C. and Hovakimyan, N., "$\mathcal{L}_1$ Adaptive Output Feedback Controller for Systems of Unknown Dimension," *IEEE Transactions on Automatic Control*, Vol. 53, No. 3, April 2008, pp. 815–821.

[35] Burl, J., "Piccolo/Piccolo Plus Autopilots - A Highly Integrated Autopilots for Small UAVs," Cloud Cap Technology, Inc., `http://cloudcaptech.com/`.

[36] Dobrokhodov, V., Kitsios, I., Kaminer, I., Jones, K., Xargay, E., Hovakimyan, N., Cao, C., Lizarraga, M., and Gregory, I., "Flight Validation of a Metrics Driven $\mathcal{L}_1$ Adaptive Control," *AIAA Guidance, Navigation, and Control Conference and Exhibit*, Honolulu, HI, August 2008.

APPENDIX

Proof of Lemma 3. We start by showing that the origin of the homogeneous equation

$$\dot{\zeta}(t) = F(t)\zeta(t)$$

is exponentially stable. To this aim, consider the Lyapunov function candidate $V_c(\zeta(t)) = \zeta^\top(t)P_c\zeta(t)$, where P_c is defined to have the same structure as in (33). Then, we have

$$\dot{V}_c(t) = \zeta^\top(t)(P_cF(t) + F^\top(t)P_c)\zeta(t)\,,$$

which yields

$$V_c(t+T) - V_c(t) \quad = \quad \int_t^{t+T} \left(\zeta^\top(\tau)(P_cF(\tau) + F^\top(\tau)P_c)\zeta(t)\right) d\tau\,.$$

Further, let $\delta_{\bar{c}}$ be a positive constant satisfying the condition

$$\delta_{\bar{c}} \;<\; \frac{1}{4}\frac{\beta}{\beta+1}\bar{\mu} \tag{76}$$

with some $\beta > 1$. Then, if we now set $\delta = \delta_{\bar{c}}$ in the definition of P_c in (33), it can be shown that for any fixed $\bar{\lambda}$ there exist arbitrarily large constant parameters a, b verifying conditions (35)-(36) with $\delta = \delta_{\bar{c}}$ and $k_c > 2$, such that for all $t \geq 0$

$$P_c \;>\; 0\,,$$

and the following inequality holds

$$\begin{aligned} V_c(t+T) \;-\; V_c(t) \;&\leq\; \int_t^{t+T} \zeta^\top(\tau)\left(P_c F(\tau) + F^\top(\tau)P_c \;+\; 2\bar{\lambda}P_c\right)\zeta(\tau)d\tau \\ &\leq\; -\int_t^{t+T} 2a\zeta_1^\top(\tau)\bar{L}(\tau)\zeta_1(\tau)d\tau \;+\; \int_t^{t+T} 2a\delta_{\bar{c}}\left\|\zeta_1(\tau)\right\|^2 d\tau \;-\; \int_t^{t+T}\frac{\delta_{\bar{c}}}{2\bar{\lambda}k_c n^3}\left\|\zeta_2(\tau)\right\|^2 d\tau \\ &=\; -\int_t^{t+T} 2a\left\|\bar{M}(\tau)\zeta_1(\tau)\right\|^2 d\tau \;+\; \int_t^{t+T} 2a\delta_{\bar{c}}\left\|\zeta_1(\tau)\right\|^2 d\tau \;-\; \int_t^{t+T}\frac{\delta_{\bar{c}}}{2\bar{\lambda}k_c n^3}\left\|\zeta_2(\tau)\right\|^2 d\tau \end{aligned} \tag{77}$$

where $\bar{M}(t)$ is such that $\bar{L}(t) = \bar{M}^\top(t)\bar{M}(t)$. These results can be easily proven using some of the derivations in Lemma 2. Next we analyze each term in the right hand-side of equation (77). The PE condition in (42) implies that

$$\frac{1}{T}\int_t^{t+T}\left\|\bar{M}(\tau)x\right\|^2 d\tau \;\;\geq\;\; \bar{\mu}\left\|x\right\|^2\,, \qquad \forall t \geq 0\,;\;\; \forall x \in \mathbb{R}^{n-1}\,,$$

and therefore, from this result, and using the dynamics of the coordination system (27) along with the relations

$$\begin{aligned} \|\zeta_1(\tau)\|^2 \;&\geq\; \frac{1}{2}\|\zeta_1(t)\|^2 - \|\zeta_1(\tau)-\zeta_1(t)\|^2 \\ \|\zeta_2(\tau)\|^2 \;&\geq\; \frac{1}{2}\|\zeta_2(t)\|^2 - \|\zeta_2(\tau)-\zeta_2(t)\|^2\,, \end{aligned}$$

it can be shown that the following inequalities hold

$$\begin{aligned}
\int_t^{t+T} \left\|\bar{M}(\tau)\zeta_1(\tau)\right\|^2 d\tau &\geq \frac{1}{2}\int_t^{t+T} \left\|\bar{M}(\tau)\zeta_1(t)\right\|^2 d\tau - \int_t^{t+T} \left\|\bar{M}(\tau)(\zeta_1(\tau)-\zeta_1(t))\right\|^2 d\tau \\
&\geq \frac{1}{2}\bar{\mu}T\left\|\zeta_1(t)\right\|^2 - a^2M^4T^2\int_t^{t+T}\left\|\bar{M}(\tau)\zeta_1(\tau)\right\|^2 d\tau - M^2T^2\int_t^{t+T}\left\|\zeta_2(\tau)\right\|^2 d\tau \quad (78)\\
\int_t^{t+T}\left\|\zeta_1(\tau)\right\|^2 d\tau &\leq 2\int_t^{t+T}\left\|\zeta_1(t)\right\|^2 d\tau + 2\int_t^{t+T}\left\|\zeta_1(\tau)-\zeta_1(t)\right\|^2 d\tau \\
&\leq 2T\left\|\zeta_1(t)\right\|^2 + 2a^2M^2T^2\int_t^{t+T}\left\|\bar{M}(\tau)\zeta_1(\tau)\right\|^2 d\tau + 2T^2\int_t^{t+T}\left\|\zeta_2(\tau)\right\|^2 d\tau \quad (79)\\
\int_t^{t+T}\left\|\zeta_2(\tau)\right\|^2 d\tau &\geq \frac{1}{2}\int_t^{t+T}\left\|\zeta_2(t)\right\|^2 d\tau - \int_t^{t+T}\left\|\zeta_2(\tau)-\zeta_2(t)\right\|^2 d\tau \\
&\geq \frac{T}{2}\left\|\zeta_2(t)\right\|^2 - \frac{b^2M^2T^2}{2}\int_t^{t+T}\left\|\bar{M}(\tau)\zeta_1(\tau)\right\|^2 d\tau\,, \quad (80)
\end{aligned}$$

where $M > \bar{M}(t)$. To prove these inequalities, we first note that

$$\zeta_1(\tau)-\zeta_1(t) = \int_t^{\tau}\dot{\zeta}_1(\sigma)d\sigma = \int_t^{\tau}\left(-a\bar{L}(\sigma)\zeta_1(\sigma)+QC\zeta_2(\sigma)\right)d\sigma\,,$$

and thus one finds

$$\begin{aligned}
\int_t^{t+T}\left\|\zeta_1(\tau)-\zeta_1(t)\right\|^2 d\tau &= \int_t^{t+T}\left\|\int_t^{\tau}\left(-a\bar{L}(\sigma)\zeta_1(\sigma)+QC\zeta_2(\sigma)\right)d\sigma\right\|^2 d\tau \\
&\leq 2\int_t^{t+T}\left(\left\|\int_t^{\tau}a\bar{L}(\sigma)\zeta_1(\sigma)d\sigma\right\|^2 + \left\|\int_t^{\tau}QC\zeta_2(\sigma)d\sigma\right\|^2\right)d\tau \\
&\leq 2\int_t^{t+T}\left(\int_t^{\tau}\left\|a\bar{L}(\sigma)\zeta_1(\sigma)\right\|d\sigma\right)^2 d\tau + 2\int_t^{t+T}\left(\int_t^{\tau}\left\|QC\zeta_2(\sigma)\right\|d\sigma\right)^2 d\tau\,.
\end{aligned}$$

Using now the Schwartz's inequality for integrals, we can write

$$\int_t^{t+T}\left\|\zeta_1(\tau)-\zeta_1(t)\right\|^2 d\tau \leq 2\int_t^{t+T}\left(\int_t^{\tau}\left\|a\bar{L}(\sigma)\zeta_1(\sigma)\right\|^2 d\sigma\int_t^{\tau}d\sigma\right)d\tau + 2\int_t^{t+T}\left(\int_t^{\tau}\left\|QC\zeta_2(\sigma)\right\|^2 d\sigma\int_t^{\tau}d\sigma\right)d\tau\,,$$

and recalling that $\|QC\| = 1$, it follows that

$$\begin{aligned}
\int_t^{t+T} \|\zeta_1(\tau) - \zeta_1(t)\|^2 d\tau &\leq 2a^2M^2 \int_t^{t+T}\int_t^{\tau} \left\|\bar{M}(\sigma)\zeta_1(\sigma)\right\|^2 d\sigma\,(\tau - t)d\tau + 2\int_t^{t+T}\int_t^{\tau} \|\zeta_2(\sigma)\|^2 d\sigma\,(\tau-t)d\tau \\
&= 2a^2M^2 \int_t^{t+T}\int_t^{\tau} \left\|\bar{M}(\sigma)\zeta_1(\sigma)\right\|^2 (\tau - t)\,d\sigma d\tau + 2\int_t^{t+T}\int_t^{\tau} \|\zeta_2(\sigma)\|^2 (\tau-t)\,d\sigma d\tau \\
&= 2a^2M^2 \int_t^{t+T}\int_\sigma^{t+T} \left\|\bar{M}(\sigma)\zeta_1(\sigma)\right\|^2 (\tau - t)\,d\tau d\sigma + 2\int_t^{t+T}\int_\sigma^{t+T} \|\zeta_2(\sigma)\|^2 (\tau-t)\,d\tau d\sigma \\
&= 2a^2M^2 \int_t^{t+T} \left\|\bar{M}(\sigma)\zeta_1(\sigma)\right\|^2 \int_\sigma^{t+T} (\tau - t)\,d\tau d\sigma + 2\int_t^{t+T} \|\zeta_2(\sigma)\|^2 \int_\sigma^{t+T} (\tau-t)\,d\tau d\sigma \\
&= 2a^2M^2 \int_t^{t+T} \left\|\bar{M}(\sigma)\zeta_1(\sigma)\right\|^2 \frac{T^2 - (\sigma-t)^2}{2} d\sigma + 2\int_t^{t+T} \|\zeta_2(\sigma)\|^2 \frac{T^2-(\sigma-t)^2}{2} d\sigma \\
&\leq a^2M^2T^2 \int_t^{t+T} \left\|\bar{M}(\sigma)\zeta_1(\sigma)\right\|^2 d\sigma + T^2 \int_t^{t+T} \|\zeta_2(\sigma)\|^2 d\sigma\,.
\end{aligned}$$

Similarly, we can prove that

$$\int_t^{t+T} \|\zeta_2(\tau) - \zeta_2(t)\|^2 d\tau \leq \frac{b^2M^2T^2}{2} \int_t^{t+T} \left\|\bar{M}(\sigma)\zeta_1(\sigma)\right\|^2 d\sigma\,.$$

Inequalities (79) and (80) follow immediately from these two results. Inequality (78) can also be easily derived from these two results noting that

$$\int_t^{t+T} \left\|\bar{M}(\tau)\left(\zeta_1(t) - \zeta_1(\tau)\right)\right\|^2 d\tau \leq M^2 \int_t^{t+T} \|\zeta_1(t) - \zeta_1(\tau)\|^2 d\tau\,.$$

Next, substituting (78), (79) and (80) into (77) yields

$$\begin{aligned}
V_c(t+T) - V_c(t) \leq\ & -\alpha_1 \|\zeta_1(t)\|^2 - \alpha_2 \|\zeta_2(t)\|^2 - \varepsilon_1 \int_t^{t+T} \left\|\bar{M}(\tau)\zeta_1(\tau)\right\|^2 d\tau - \varepsilon_2 \int_t^{t+T} \|\zeta_2(\tau)\|^2 d\tau \\
&+ \frac{1}{\beta}\left(\int_t^{t+T} 2a \left\|\bar{M}(\tau)\zeta_1(\tau)\right\|^2 d\tau + \int_t^{t+T} 2a\delta_{\bar{c}} \|\zeta_1(\tau)\|^2 d\tau - \int_t^{t+T} \frac{\delta_{\bar{c}}}{2\bar{\lambda}k_c n^3} \|\zeta_2(\tau)\|^2 d\tau\right),
\end{aligned}$$

where $\beta > 1$ was introduced in (76) and

$$\begin{aligned}
\alpha_1 &= a\bar{\mu}T - 4\frac{\beta+1}{\beta} a\delta_{\bar{c}} T \\
\alpha_2 &= \frac{1}{4}\frac{\delta_{\bar{c}}}{\bar{\lambda}k_c n^3} T \\
\varepsilon_1 &= \frac{2a}{\beta} - \left(2a^3M^4 + 4\frac{\beta+1}{\beta}\delta_{\bar{c}}a^3M^2 + \frac{1}{4}\frac{\delta_{\bar{c}}}{\bar{\lambda}k_c n^3} b^2M^2\right) T^2 \\
\varepsilon_2 &= \frac{1}{\beta}\frac{\delta_{\bar{c}}}{2\bar{\lambda}k_c n^3} - \left(2aM^2 + 4\frac{\beta+1}{\beta}\delta_{\bar{c}}a\right) T^2\,.
\end{aligned}$$

It is easy to check that the condition (76) leads to $\alpha_1 > 0$. For sufficiently small time T, it follows that $\varepsilon_1,\, \varepsilon_2 > 0$, and then one can write

$$V_c(t+T) - V_c(t) \;\leq\; -\alpha_1 \left\|\zeta_1(t)\right\|^2 \;-\; \alpha_2 \left\|\zeta_2(t)\right\|^2 \;-\; \frac{1}{\beta}\left(V_c(t+T) - V_c(t)\right)\,,$$

where we have used the inequality (77).

Consequently, for any $t \geq 0$, we have

$$V_c(t+T) - V_c(t) \;\leq\; -\frac{\beta}{\beta+1}\left(\alpha_1 \left\|\zeta_1(t)\right\|^2 \;+\; \alpha_2 \left\|\zeta_2(t)\right\|^2\right)\,,$$

and therefore there exists $\bar{\alpha}$, satisfying $0 < \bar{\alpha} < 1$, such that

$$V_c(t+T) - V_c(t) \;\leq\; -\bar{\alpha} V_c(t)\,.$$

We thus conclude that

$$V_c(t+T) \;\leq\; (1-\bar{\alpha})\, V_c(t) \;\leq\; \alpha V_c(t) \tag{81}$$

where the constant α satisfies $0 < \alpha < 1$. Applying now (81) successively we obtain for $t = (k-1)T$

$$V_c(t) \leq V_c(kT) \leq \alpha^k V_c(0), \qquad \forall t \geq kT\,, \quad k = 0, 1, \ldots$$

Thus, $V_c(t)$ and consequently $\zeta(t)$ converge exponentially fast to zero as $t \to \infty$. From this and the fact that the forced system (31) is linear and $L(t)$ is bounded, it follows that the ISS bound (28) holds (see Ref. [26]). Then, as we showed in Lemma 2, inequalities (29) and (30) also hold. □

Proof of Lemma 6. First we recall from Lemma 1 that, if $x_i(t) \in \bar{\Omega}$ for all $t \in [0, \tau]$, then one finds that

$$\begin{array}{lcllcl} |x_{F_i}(t)| & \leq & d & |\theta_{e_i}(t)| & \leq & \nu_1 \\ |y_{F_i}(t)| & \leq & d & |\psi_{e_i}(t)| & \leq & \nu_2 \\ |z_{F_i}(t)| & \leq & d\,, & & & \end{array} \tag{82}$$

and also that

$$|\theta_{e_i}(t) - \delta_{\theta_i}(t)| \;\leq\; \sqrt{cc_2}\,, \qquad |\psi_{e_i}(t) - \delta_{\psi_i}(t)| \;\leq\; \sqrt{cc_2}\,, \tag{83}$$

which holds for any $t \in [0, \tau]$.

In preparation for the development that follows, next we introduce the following notation: let

$$\epsilon_0 \;=\; \frac{v_{\max}\cos\nu_1\cos\nu_2 - v_{d_1}\frac{l_{f_{\max}}}{l_{f_1}} - K_1 d - \bar{\bar{k}}_1\beta_0 l_{f_{\max}}}{\cos\nu_1\cos\nu_2 \;+\; \bar{\bar{k}}_2 l_{f_{\max}}}\,, \tag{84}$$

where $\bar{\bar{k}}_1 = (2a(n-1)+1)k_1$ and $\bar{\bar{k}}_2 = (2a(n-1)+1)k_2$, and β_0 was introduced in condition (59), which ensures that $\epsilon_0 > 0$. Further, let ϵ be defined as

$$0 \;<\; \epsilon \;<\; \epsilon_0\,, \tag{85}$$

and define

$$v_{c_{\max}} \;=\; v_{\max} - \epsilon\,.$$

It is easy to check from the definition of ϵ_0 in (84) and the choice of ϵ in (85) that $v_{c_{\max}} > 0$. In fact,

$$\begin{aligned} v_{\max} - \epsilon \;&>\; v_{\max} - \epsilon_0 \\ &=\; v_{\max} - \frac{v_{\max}\cos\nu_1\cos\nu_2 - v_{d_1}\frac{l_{f_{\max}}}{l_{f_1}} - K_1 d - \beta_0 l_{f_{\max}}}{\cos\nu_1\cos\nu_2 \;+\; \bar{\bar{k}}_2 l_{f_{\max}}} \\ &>\; v_{\max} - \frac{v_{\max}\cos\nu_1\cos\nu_2}{\bar{\bar{k}}_2 l_{f_{\max}} + \cos\nu_1\cos\nu_2} \\ &>\; v_{\max} - v_{\max} \;=\; 0\,. \end{aligned}$$

Further, let

$$\gamma_{\dot{v}_c} = \frac{\left(\bar{k}_3\beta_0 + \bar{k}_4\epsilon_0 + K_1\dot{x}_{F_{\max}}\right) + \left(\bar{\bar{k}}_1\beta_0 + \bar{\bar{k}}_2\epsilon_0 + \frac{v_{d_1}}{l_{f_1}}\right)\left(\dot{\theta}_{e_{\max}}\sin\nu_1 + \dot{\psi}_{e_{\max}}\sin\nu_2\right)}{\cos^2\nu_1\cos^2\nu_2} + \epsilon_1 \tag{86}$$

where $\bar{k}_3 = 2(n-1)(a\bar{k}_1 + bk_1)$, $\bar{k}_4 = 2(n-1)(a\bar{k}_2 + bk_2)$, $\bar{k}_1 = (2a(n-1)+1)k_1$, $\bar{k}_2 = (2a(n-1)+1)k_2 + \frac{1}{l_{f_{\min}}}$, ϵ_1 is an arbitrarily small positive constant, and $\dot{x}_{F_{\max}}$, $\dot{\theta}_{e_{\max}}$, and $\dot{\psi}_{e_{\max}}$ are defined as

$$\begin{aligned}
\dot{x}_{F_{\max}} &= (K_1 d + v_{\max})(1 + \kappa_{\max} d) + v_{\max} \\
\dot{\theta}_{e_{\max}} &= (K_1 d + V_{\max})\,\zeta_{\max} + (\gamma_{q_c} + \bar{\gamma}_\theta) + (\gamma_{r_c} + \bar{\gamma}_\psi) \\
\dot{\psi}_{e_{\max}} &= (K_1 d + V_{\max})(\zeta_{\max}\tan\nu_1 + \kappa_{\max}) + \frac{(\gamma_{q_c} + \bar{\gamma}_\theta) + (\gamma_{r_c} + \bar{\gamma}_\psi)}{\cos\nu_1},
\end{aligned}$$

with

$$\gamma_{q_c} = \gamma_{r_c} = u_{\theta_{c\max}} + u_{\psi_{c\max}} + (K_1 d + v_{\max})\,\zeta_{\max}\sin\nu_2 + (K_1 d + v_{\max}(\zeta_{\max}\tan\nu_1 + \kappa_{\max})), \tag{87}$$

and

$$\begin{aligned}
u_{\theta_{c\max}} &= K_2\sqrt{cc_2} + \frac{c_2}{c_1}dv_{\max} + \frac{1}{d_1\sqrt{1 + \left(\frac{d}{d+d_1}\right)^2}}\left((K_1 d + v_{\max})\,\zeta_{\max} d + v_{\max}\sin\nu_1\right) \\
u_{\psi_{c\max}} &= K_3\sqrt{cc_2} + \frac{c_2}{c_1}dv_{\max} + \frac{1}{d_2\sqrt{1 + \left(\frac{d}{d+d_2}\right)^2}}\left((K_1 d + v_{\max})(\zeta_{\max} + \kappa_{\max})\,d + v_{\max}\sin\nu_2\right),
\end{aligned}$$

while $\bar{\gamma}_\theta$ and $\bar{\gamma}_\psi$ are some arbitrarily small positive constants.

Let $t_{s1} \in [0, \tau]$ be the first time at which the communication topology switches. Next we show by contradiction that

$$\|(v_{c_i})_{t_{s1}}\|_{\mathcal{L}_\infty} < v_{c_{\max}} \tag{88}$$
$$\|(\dot{v}_{c_i})_{t_{s1}}\|_{\mathcal{L}_\infty} < \gamma_{\dot{v}_c}. \tag{89}$$

Since $v_{c_i}(0) < v_{c_{\max}}$ and $|\dot{v}_{c_i}(0)| < \gamma_{\dot{v}_c}$ by assumption, and both $v_{c_i}(t)$ and $\dot{v}_{c_i}(t)$ are continuous and differentiable for all $t \in [0, t_{s1}^-]$, if (88) or (89) are not true, then there exist a time $t^* \in [0, t_{s1}^-]$ such that either

$$v_{c_i}(t^*) = v_{c_{\max}} \tag{90}$$

or

$$|\dot{v}_{c_i}(t^*)| = \gamma_{\dot{v}_c}, \tag{91}$$

while

$$\begin{aligned}
v_{c_i}(t) &< v_{c_{\max}} \\
|\dot{v}_{c_i}(t)| &< \gamma_{\dot{v}_c},
\end{aligned}$$

for all $t \in [0, t^*)$.

If the initial condition in speed satisfies the bound in (60), Lemma 4 ensures that

$$\|(v_{c_i} - v_i)_{t^*}\|_{\mathcal{L}_\infty} \leq \gamma_{v_i}, \tag{92}$$

where γ_{v_i} can be rendered arbitrarily small by increasing the adaptation gain Γ_c and the bandwidths of the low-pass filter ω_v and the reference model m_v. In particular, we choose the adaptation gain Γ_c, ω_v and m_v so that $\bar{\gamma}_v = \max\{\gamma_{v_1}, \ldots, \gamma_{v_n}\}$ verifies the following condition

$$\bar{\gamma}_v < \epsilon. \tag{93}$$

Then it follows that

$$\|(v_i)_{t^*}\|_{\mathcal{L}_\infty} \;\leq\; \|(v_{c_i})_{t^*}\|_{\mathcal{L}_\infty} \;+\; \gamma_{v_i} \;\leq\; v_{c_{\max}} + \gamma_{v_i} \;\leq\; v_{c_{\max}} + \bar{\gamma}_v \;=\; v_{\max} - (\epsilon - \bar{\gamma}_v) \;<\; v_{\max}\,,$$

and all conditions of Lemma 5 hold, which implies that

$$\begin{array}{rclcrcl} \|q_{c_i}\|_{\mathcal{L}_\infty} & \leq & \gamma_{q_c}\,, & & \|\dot{q}_{c_i}\|_{\mathcal{L}_\infty} & \leq & \gamma_{\dot{q}_c} \\ \|r_{c_i}\|_{\mathcal{L}_\infty} & \leq & \gamma_{r_c}\,, & & \|\dot{r}_{c_i}\|_{\mathcal{L}_\infty} & \leq & \gamma_{\dot{r}_c}\,, \end{array} \tag{94}$$

where γ_{q_c} and γ_{r_c} were defined in (87), while $\gamma_{\dot{q}_c}$ and $\gamma_{\dot{r}_c}$ are some positive constants. From this result and the bounds on the initial conditions in (60) it follows that

$$\|(q_{c_i} - q_i)_{t^*}\|_{\mathcal{L}_\infty} \;\leq\; \gamma_{\theta_i} \tag{95}$$

$$\|(r_{c_i} - r_i)_{t^*}\|_{\mathcal{L}_\infty} \;\leq\; \gamma_{\psi_i}\,. \tag{96}$$

In particular, we choose the adaptation gain Γ_c, ω_q, m_q, ω_r, and m_r so that

$$\begin{array}{rcll} \gamma_{\theta_i} & < & \bar{\gamma}_\theta & \\ \gamma_{\psi_i} & < & \bar{\gamma}_\psi\,, & i = 1, \ldots, n\,. \end{array}$$

Next, we analyze separately the two cases (90) and (91).

1. So assume first that (90) occurs. It follows from Lemmas 2 and 3, and the bound in (92) that

$$\left\|\left(l_i' - l_j'\right)_{t^*}\right\|_{\mathcal{L}_\infty} \;\leq\; 2k_1\,\|\zeta(0)\| \;+\; 2k_2\bar{\gamma}_v \tag{97}$$

$$\begin{aligned} \left\|\left(\dot{l}_i' - \frac{v_{d_1}}{l f_1}\right)_{t^*}\right\|_{\mathcal{L}_\infty} &\leq a(n-1)\left(2k_1\,\|\zeta(0)\| \;+\; 2k_2\bar{\gamma}_v\right) \;+\; \left(k_1\,\|\zeta(0)\| \;+\; k_2\bar{\gamma}_v\right) \;+\; \frac{\bar{\gamma}_v}{l_{f_{\min}}} \\ &= \underbrace{\left(2a(n-1)k_1 + k_1\right)}_{\bar{k}_1}\|\zeta(0)\| \;+\; \underbrace{\left(2a(n-1)k_2 + k_2 + \frac{1}{l_{f_{\min}}}\right)}_{\bar{k}_2}\bar{\gamma}_v\,. \end{aligned} \tag{98}$$

This implies that

$$\begin{aligned} \|(u_{\mathrm{coord}_i})_{t^*}\|_{\mathcal{L}_\infty} &\leq a(n-1)\left(2k_1\,\|\zeta(0)\| \;+\; 2k_2\bar{\gamma}_v\right) \;+\; \frac{v_{d_1}}{l_{f_1}} \;+\; \left(k_1\,\|\zeta(0)\| \;+\; k_2\bar{\gamma}_v\right) \\ &= \underbrace{\left(2a(n-1)k_1 + k_1\right)}_{\bar{\bar{k}}_1}\|\zeta(0)\| \;+\; \underbrace{\left(2a(n-1)k_2 + k_2\right)}_{\bar{\bar{k}}_2}\bar{\gamma}_v \;+\; \frac{v_{d_1}}{l_{f_1}}\,, \end{aligned}$$

which yields

$$\|(v_{c_i})_{t^*}\|_{\mathcal{L}_\infty} \;\leq\; \frac{\left(\bar{\bar{k}}_1\,\|\zeta(0)\| + \bar{\bar{k}}_2\bar{\gamma}_v + \frac{v_{d_1}}{l_{f_1}}\right) l_{f_i} + K_1 d}{\cos\nu_1\cos\nu_2}\,.$$

From condition (59), the design constraint in (93), and the definition of ϵ_0 in (84), it follows that

$$\begin{aligned} \|(v_{c_i})_{t^*}\|_{\mathcal{L}_\infty} &\leq \frac{\left(\bar{\bar{k}}_1\beta_0 + \bar{\bar{k}}_2\bar{\gamma}_v + \frac{v_{d_1}}{l_{f_1}}\right) l_{f_i} + K_1 d}{\cos\nu_1\cos\nu_2} \\ &\leq \frac{\left(\bar{\bar{k}}_1\beta_0 + \bar{\bar{k}}_2\epsilon_0 + \frac{v_{d_1}}{l_{f_1}}\right) l_{f_{\max}} + K_1 d}{\cos\nu_1\cos\nu_2} \\ &= v_{\max} - \epsilon_0 \\ &< v_{\max} - \epsilon \;=\; v_{c_{\max}}\,, \end{aligned}$$

which contradicts the assumption in (90).

2. Next we derive a contradicting argument to (91). The derivative of $v_c(t)$ is given by

$$\dot{v}_{c_i} = \frac{(\dot{u}_{\text{coord}_i} l_{f_i} - K_1 \dot{x}_{F_i}) \cos\theta_{e_i} \cos\psi_{e_i} + (u_{\text{coord}_i} l_{f_i} - K_1 x_{F_i}) \left(\dot{\theta}_{e_i} \sin\theta_{e_i} \cos\psi_{e_i} + \dot{\psi}_{e_i} \cos\theta_{e_i} \sin\psi_{e_i}\right)}{\cos^2\theta_{e_i} \cos^2\psi_{e_i}}$$

where

$$\dot{u}_{\text{coord}_i} = -\sum_{j\in J_i} a\left(l_i' - l_j'\right) - \sum_{j\in J_i} b\left(l_i' - l_j'\right) .$$

It follows from the dynamics in (9) and the bounds in (82) that

$$\begin{aligned}
\|(\dot{x}_{F_i})_{t^*}\|_{\mathcal{L}_\infty} &\leq (K_1 d + v_{\max})(1 + \kappa_{\max} d) + v_{\max} = \dot{x}_{F_{\max}} \\
\left\|(\dot{\theta}_{e_i})_{t^*}\right\|_{\mathcal{L}_\infty} &\leq (K_1 d + V_{\max})\,\zeta_{\max} + (\gamma_{q_c} + \gamma_{\theta_i}) + (\gamma_{r_c} + \gamma_{\psi_i}) \leq \dot{\theta}_{e_{\max}} \\
\left\|(\dot{\psi}_{e_i})_{t^*}\right\|_{\mathcal{L}_\infty} &\leq (K_1 d + V_{\max})(\zeta_{\max}\tan\nu_1 + \kappa_{\max}) + \frac{(\gamma_{q_c} + \gamma_{\theta_i}) + (\gamma_{r_c} + \gamma_{\psi_i})}{\cos\nu_1} \leq \dot{\psi}_{e_{\max}} .
\end{aligned}$$

Further, from the bound in (98), we find

$$\begin{aligned}
\left\|\left(l_i' - l_j'\right)_{t^*}\right\|_{\mathcal{L}_\infty} &\leq \left\|\left(\left(l_i' - \frac{v_{d_1}}{l_{f_1}}\right) - \left(l_j' - \frac{v_{d_1}}{l_{f_1}}\right)\right)_{t^*}\right\|_{\mathcal{L}_\infty} \\
&\leq \left\|\left(l_i' - \frac{v_{d_1}}{l_{f_1}}\right)_{t^*}\right\|_{\mathcal{L}_\infty} + \left\|\left(l_j' - \frac{v_{d_1}}{l_{f_1}}\right)_{t^*}\right\|_{\mathcal{L}_\infty} \\
&\leq 2\bar{k}_1 \|\zeta(0)\| + 2\bar{k}_2\bar{\gamma}_v .
\end{aligned}$$

From this result and the bound in (97) it follows that

$$\begin{aligned}
\|(\dot{u}_{\text{coord}_i})_{t^*}\|_{\mathcal{L}_\infty} &\leq a(n-1)\left(2\bar{k}_1\|\zeta(0)\| 2\bar{k}_2\bar{\gamma}_v\right) + b(n-1)\left(2k_1\|\zeta(0)\| 2k_2\bar{\gamma}_v\right)\bar{\gamma}_v \\
&= \underbrace{2(n-1)\left(a\bar{k}_1 + bk_1\right)}_{\bar{k}_3}\|\zeta(0)\| + \underbrace{2(n-1)\left(a\bar{k}_2 + bk_2\right)}_{\bar{k}_4}\bar{\gamma}_v ,
\end{aligned}$$

which leads to the following bound

$$\|(\dot{v}_{c_i})_{t^*}\|_{\mathcal{L}_\infty} \leq \frac{\left(\bar{k}_3\|\zeta(0)\| + \bar{k}_4\bar{\gamma}_v + K_1\dot{x}_{F_{\max}}\right) + \left(\bar{\bar{k}}_1\|\zeta(0)\| + \bar{\bar{k}}_2\bar{\gamma}_v + \frac{v_{d_1}}{l_{f_1}}\right)\left(\dot{\theta}_{e_{\max}}\sin\nu_1 + \dot{\psi}_{e_{\max}}\sin\nu_2\right)}{\cos^2\nu_1\cos^2\nu_2} ,$$

and from the definition of $\gamma_{\dot{v}_c}$ in (86) it follows that

$$\|(\dot{v}_{c_i})_{t^*}\|_{\mathcal{L}_\infty} \leq \gamma_{\dot{v}_c} - \epsilon_1 < \gamma_{\dot{v}_c} ,$$

which contradicts the assumption in (91).

Since (90) and (91) are not true, the relationships in (88) and (89) hold for all $t \in [0, t_{s1}^-]$.

Next we show that the same bounds hold also for all $t \in [t_{s1}^+, \tau]$. To this aim, we prove that, under the assumptions of the Lemma, the bounds on the initial conditions at $t = 0$ that helped us prove the bounds on $v_{c_i}(t)$ and $\dot{v}_{c_i}(t)$ for the time interval $t \in [0, t_{s1}^-]$ hold also at the switching time $t = t_{s1}$ and by extension to all switching times $t = t_s$.

From the bounds in (60) it follows that

$$\left|v_{c_i}(t_{s1}^+) - v_i(t_{s1})\right| \leq \bar{\gamma}_v$$

Further, by continuity of $v_i(t)$, we have the the bounds in (94), (95), and (96) hold also for $t = t_{s1}^+$. Therefore, we can write

$$v_{c_i}(t_{s1}^+) \leq \frac{\left(\bar{\bar{k}}_1 \left\|\zeta(0)\right\| \mathrm{e}^{-\bar{\lambda} t_{s1}} + \bar{\bar{k}}_2 \bar{\gamma}_v + \frac{v_{d_1}}{l_{f_1}}\right) l_{f_i} + K_1 d}{\cos\nu_1 \cos\nu_2}$$

and

$$|\dot{v}_c(t_{s1})| \leq \frac{\left(\bar{k}_3 \left\|\zeta(0)\right\| \mathrm{e}^{-\bar{\lambda} t_{s1}} + \bar{k}_4 \bar{\gamma}_v + K_1 \dot{x}_{F_{\max}}\right) + \left(\bar{\bar{k}}_1 \left\|\zeta(0)\right\| \mathrm{e}^{-\bar{\lambda} t_{s1}} + \bar{\bar{k}}_2 \bar{\gamma}_v + \frac{v_{d_1}}{l_{f_1}}\right) \left(\dot{\theta}_{e_{\max}} \sin\nu_1 + \dot{\psi}_{e_{\max}} \sin\nu_2\right)}{\cos^2\nu_1 \cos^2\nu_2},$$

which implies that

$$\begin{aligned} v_{c_i}(t_{s1}^+) &< v_{c_{\max}} \\ |\dot{v}_{c_i}(t_{s1})| &< \gamma_{\dot{v}_c}\,. \end{aligned}$$

These two bounds together with the bound in the initial condition in (60) ensure that the bounds in (88) and (89) hold also for the time interval $t \in [t_{s1}, t_{s2}]$. By repeating the same procedure again and again, we can extend the result to the whole interval $t \in [0, \tau]$. This concludes the proof. □

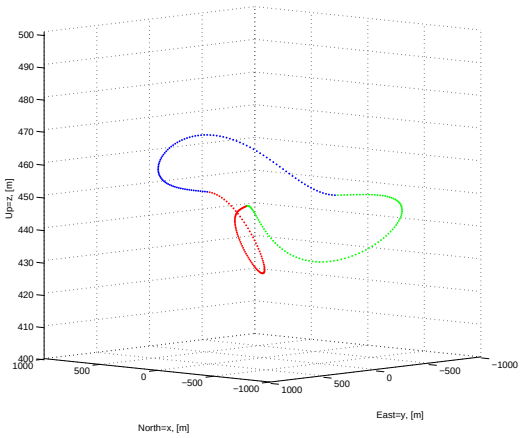

(a) Spatial deconfliction ($d_{\min} = 100$ m)

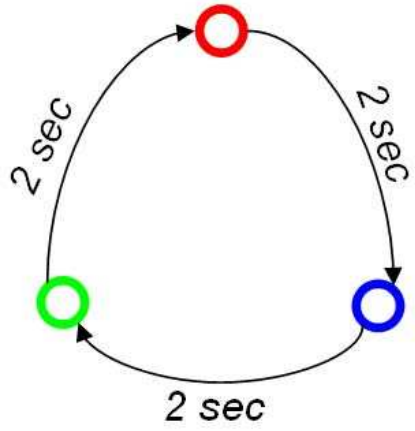

(b) Time-varying communication topology

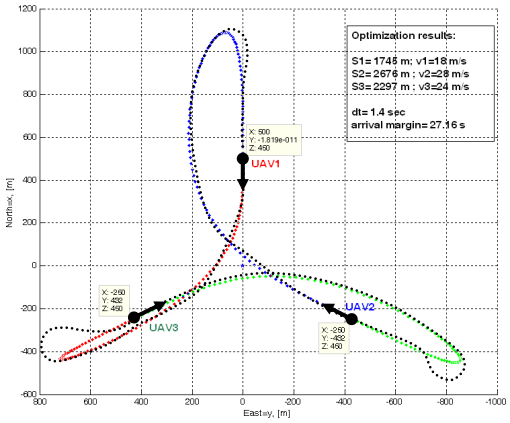

(c) Coordinated path tracking (2D projection).

Figure 13: HIL'08. Coordinated path following of 3 UAVs.